Review

Solvothermal Synthesis of Multifunctional Coordination Polymers

Yonggang Zhao, Kunhao Li, and Jing Li

Department of Chemistry and Chemical Biology, Rutgers University, Piscataway, NJ 08854, USA

Reprint requests to Prof. Dr. Jing Li. Fax: 732-445-5312. E-mail: jingli@rutgers.edu

Z. Naturforsch. **2010**, *65b,* 976 – 998; received March 31, 2010

This review focuses primarily on the past 10 years of our development of multifunctional coordination polymers with 1D, 2D and 3D structures employing low-temperature and cost-effective hydrothermal and solvothermal methods. The effects of the experimental conditions and parameters on the crystal formation and phase separation, including temperature and pressure, reaction pH, solvent and composition, are discussed. Our studies have shown that a variety of different types of network structures may be rationally designed and synthesized by deliberate selection and construction of metal building blocks and organic ligands, which lead to numerous interesting properties and multifunctionality that are promising for applications in gas storage and separation, catalysis and optical sensing.

Key words: Solvothermal Synthesis, Coordination Polymer, Metal-Organic Framework, Porosity, Multifunctionality

Introduction

Coordination polymers: Background and history

As one of the most attractive and challenging research areas of chemistry and material science, the study of novel coordination polymers, also referred as metal-organic frameworks (MOFs), is undergoing a burgeoning development [1 – 7]. Coordination polymers are known as compounds containing both inorganic units and organic ligands as integral parts which extend to one-, two- and three-dimensional infinite networks through coordinative bonding connectivity [8 – 10]. As a rule, coordination polymers are solids. The structural features of these solid-state materials are typically governed by three aspects: the connectors (metal or metal clusters); linkers (ligand molecules); and their connectivity. Many intriguing properties of these materials rely on their structures and topology. Thus by employing well-chosen starting materials, coordination polymers possessing fascinating structures and interesting properties can be rationally and deliberately designed and synthesized. To date, much work in this field has demonstrated that the tailoring nature of structures and functionalities has made coordination polymers promising candidates in various applications, including adsorption,

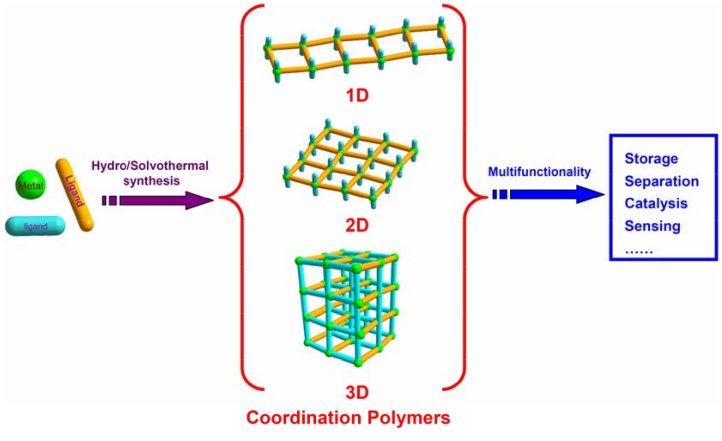

separation, catalysis, magnetism, sensing, and host-guest chemistry [11 – 14].

While the term "coordination polymer" was first introduced a long time ago in the early 1960s [15], strong interests began to grow only after 30 years, bringing together researchers across the world to work in this field. Robson and coworkers [16, 17] delineated principles of coordination polymers and extrapolated Wells' work [18] to infinite metal organic frameworks. Later on, Zaworotko [19, 20], Fujita [21, 22], Kitagawa [23 – 25], Férey [26, 27] and others contributed to expand the structure database by using net-based approach. Studies by Yaghi and coworkers revealed the tremendous potential in adsorption-related applications of open framework coordination polymers, or porous metal-organic frameworks, and illustrated the strategies for construction of MOFs with control of their vertex geometry, functionality, and pore characteristics, giving a leap in accelerating the pace of development [28 – 31]. Since the 1990s, thousands of publications on this remarkable class of materials have appeared.

Coordination polymers: Synthesis and crystal growth

Among numerous synthetic methods and techniques used for the preparation of solid materials, solvothermal/hydrothermal methods have been confirmed to be among the most effective and convenient routes under relatively mild conditions, in particular for the crystal growth of coordination polymers [32 – 34]. Solvothermal reactions involve the use of an organic or inorganic solvent at elevated temperature and autogeneous pressure in a sealed system (usually Teflon-lined autoclaves or glass vials) [35]. When water is used as the solvent, the reactions are referred to as hydrothermal. Solvents, under such subcritical and supercritical conditions, undergo a dramatic change in many of their properties, such as density, viscosity, and diffusion coefficient, *etc.* Consequently, the diffusion and reactivity of chemical species are greatly enhanced, and many reactions can occur at much lower temperatures.

For the determination of the topology, dimensionality and porosity of coordination polymers, obtaining high-quality single crystals suitable for X-ray diffraction analysis has become essential. While the solvothermal process has been found to be an efficient solution to the problems often encountered in the crystal growth using traditional solution or diffusion methods [36], a successful synthesis of a targeted coordination polymer will depend largely on the experimental conditions. Many reaction parameters need to be considered, including composition of the reactants, temperature and pressure, concentration, reaction time, pH value and solubility, to name a few [37]. As the crystallization under solvothermal conditions is often a non-equilibrium process and may give rise to metastable products, the cooling rate at the end of the reaction is also an important parameter to take into consideration. Selection of the solvent is very important, since some metal salts and/or organic ligands have very low solubility or are even insoluble in a given solvent. In some cases, introducing two or three solvents and ultrasonic pretreatment may be helpful to increase solubility. Moreover, solvents play crucial roles as the structure directing, templating, and pore-filling agents during the formation of coordination polymers.

This review does not intend to give a comprehensive coverage of the coordination polymers synthesized by solvo(hydro)thermal methods. Rather, it will focus mainly on our own contributions using this approach over the past decade, and on the relationships between the synthesis, the crystal and pore structures and the functionality of these materials.

Solvo(hydro)thermal Synthesis of Selected Compounds

Hydrothermal reactions

Our early work had centered on the design and preparation of coordination polymers by employing hydrothermal reactions. In the case of the formation of one-dimensional Cu-dpa (dpa = 2,2′-dipyridylamine) structures, the stoichiometry of the starting materials was the most important parameter affecting the final products [38]. Heating a mixture of $CuCl_2 \cdot 2H_2O$ (0.1705 g) and dpa (0.1712 g) at 1 : 1 ratio in H_2O (5 mL) in an acid digestion bomb at 170 °C afforded the compound $[(CuCl)_2(dpiz)]$ (**1**) as orange crystals. Structure analysis has revealed that the dpa ligand was rearranged to give rise to the formation of dpiz ([1,2-a : 2′,3′-d]imidazole) *in situ* during the hydrothermal process (Scheme 1), in which the 1D Cu-dipz-halide polymer was formed (Fig. 1a). In compound **1**, Cu(1) and Cu(2), having different coordination configuration, are connected and extend to one-dimensional chains

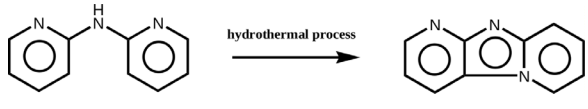

Scheme 1.

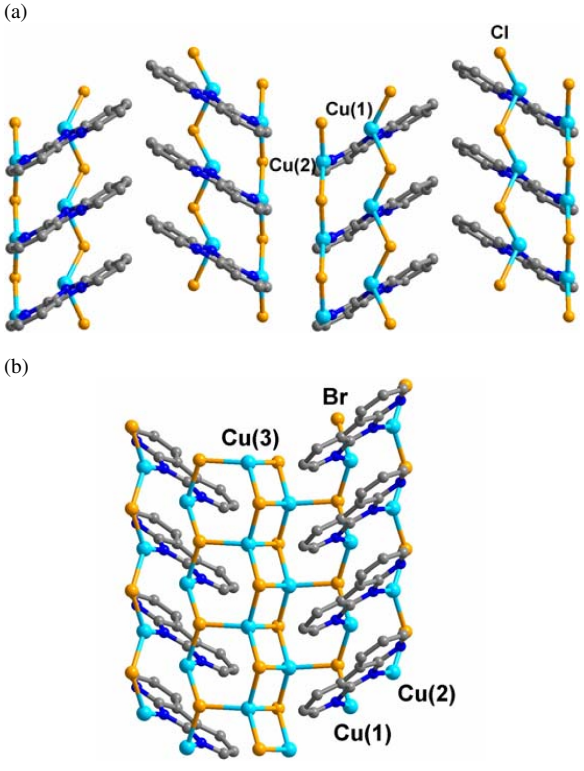

Fig. 1 (color online). Perspective view of the one-dimensional chain structures of compounds **1** (a, view along the *b* axis) and **2** (b, view along the *c* axis). Cu (turquoise), Cl/Br (orange), N (blue) and C (gray).

via μ_2-Cl and μ_3-Cl atoms. However, using the same experimental condition, the reaction of $CuBr_2$, dpa and H_2O in a molar ration of 2 : 1 : 334 gave orange crystals of the compound $[(CuBr)_3(dpiz)]$ (**2**). The structure of compound **2** is in part similar to that of compound **1** but an additional infinite Cu_2Br_2 zigzag double chain is found between every other pair of $(CuBr)_2(dpiz)$ chains to give a one-dimensional ribbon-like structure (Fig. 1b). The three chains are connected *via* Cu(3)-(μ_2-Br) bonds, where Cu(3) is the third crystallographically independent copper site in this structure. The reactions of compounds **1** and **2** involved reduction of Cu(II) to Cu(I) and chemical rearrangement of dpa to dpiz, which was stimulated under the hydrothermal conditions. This study was one of the very first examples of the solvo(hydro)thermal synthesis of coordination polymers featuring one-pot and *in situ* ligand generation.

Compound $[(CuBr)_2bpy]$ (**3**) (bpy = 4,4′-bipyridine) was prepared by the reaction of $CuBr_2$ and bpy in water with the molar ratio being 1 : 1 : 167. The mixture was loaded in a 23 mL acid digestion bomb and heated at 170 °C for 7 d to yield dark-yellow crystals [39]. Compound **3** consists of the aforementioned Cu_2X_2 zigzag double chains shown in compound **2** (Fig. 2a). These Cu_2X_2 chains are further connected by bpy ligands to form two-dimensional layers in the *ab* plane.

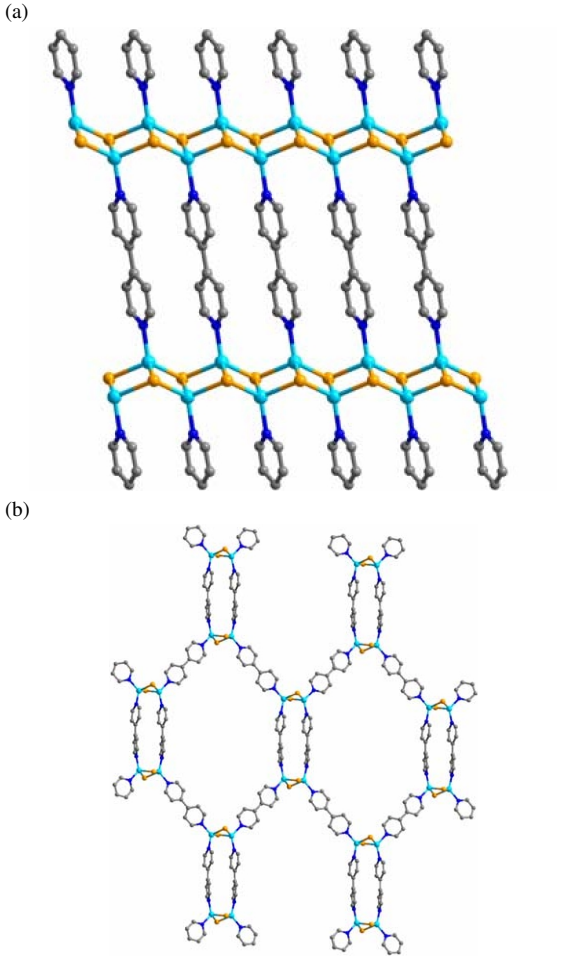

Fig. 2 (color online). a) Perspective view of the two-dimensional layer in compound **3** along the *c* axis; b) structure of the interlocking planar net in **4**. The octagonal ring is shown in the center. Cu (turquoise), Br (orange), N (blue) and C (gray).

Increasing the amount of bpy by a factor of 2 against copper bromide (to the 2 : 1 ratio) while keeping other experimental conditions unchanged produced compound [CuBr(bpy)] (**4**) in quantitative yield. The structure of compound **4** consists of four-fold interlocking planar 2D nets, which interpenetrate each other to give a three-dimensional framework structure (Fig. 2b). The planar networks are composed of large octagonal

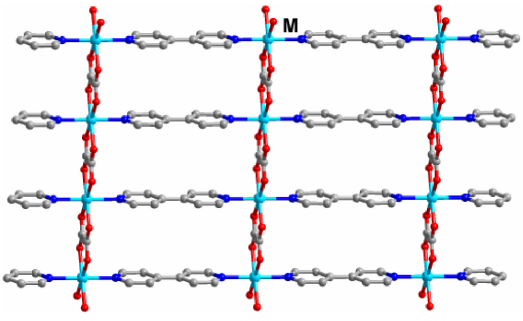

Fig. 3 (color online). Two-dimensional network of compounds **5**–**8** viewed along the *c* axis. *M* = Fe, Co, Ni and Zn (turquoise), O (red), N (blue) and C (gray).

rings, formed by sharing bpy ligands and rectangular $[(Cu_2Br_2)(bpy)]_2$ units. In compound **4**, the stoichiometry has turned to $Cu_2Br_2(bpy)_2$.

Compounds **5**–**8** with the general formula $[M(ox)(bpy)]$ (*M* = Fe(II), (**5**); Co(II), (**6**); Ni(II), (**7**); Zn(II), (**8**); ox = $C_2O_4^{2-}$) belong to a family of mixed-ligand coordination polymers having two-dimensional layered structures [40]. The general preparation procedure of compounds **5**–**8** is described below. The mixture of MX_2 (*X* = Br or Cl), oxalic acid and bpy in the molar ratio of 1 : 1 : 1 in 4 mL of H_2O (8 mL for Zn) was sealed in a 23 mL acid digestion bomb and heated at 170 °C for 7 d. The crystals of the product were isolated by filtration and washed with water and acetone, then dried in air. X-Ray diffraction analysis has shown that the metal atoms are all six-coordinated to four oxygen atoms from oxalate ions and two nitrogen atoms from bpy ligands, forming a strictly rectangular grid in the *ab* plane (Fig. 3). Adjacent layers stack on top of each other in a staggered fashion to complete the structure in the third dimension. Experiments show that the hydrothermal conditions are crucial for the formation and crystallization of compounds **5**–**8**, since syntheses using H_2O and other organic solvents all led to different products. The results of our study also indicate that the pH value of the solution will affect the crystallinity of products.

Three isostructural two-dimensional coordination polymers $[MCl_2(bpy)]$ [*M* = Fe(II), (**9**); Co(II), (**10**); Ni(II), (**11**)] were crystallized *via* the hydrothermal method (Fig. 4) [41]. Crystals or polycrystalline samples of **9**–**11** were obtained by heating the mixtures of MCl_x (*M* = Fe, Co, Ni, 1 mmol, for Fe, *x* = 2 or 3; for Co or Ni, *x* = 2), $H_2C_2O_4 \cdot 2H_2O$ (1 mmol), bpy (1 mmol) and H_2O (5 mL) in 23 mL acid digestion bombs at 170 °C for 7 d. In compounds **9**–**11**, metal

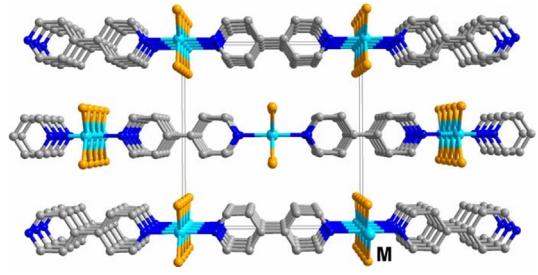

Fig. 4 (color online). Two-dimensional networks of compounds **9**–**11** viewed along the *b* axis. *M* = Fe, Co and Ni (turquoise), Cl (orange), N (blue), C (gray).

ions having octahedral coordination geometry are bridged by μ_2-Cl to form 1D chains extending along the *c* direction. These chains are interlinked by bpy ligands to form 2D layered networks in the *ac* plane. The M–M distances are in the range 3.58–3.62 Å.

Compared with the more extensively studied transition metal coordination polymers, rare earth metal coordination network compounds are relatively un-

(a)

(b)

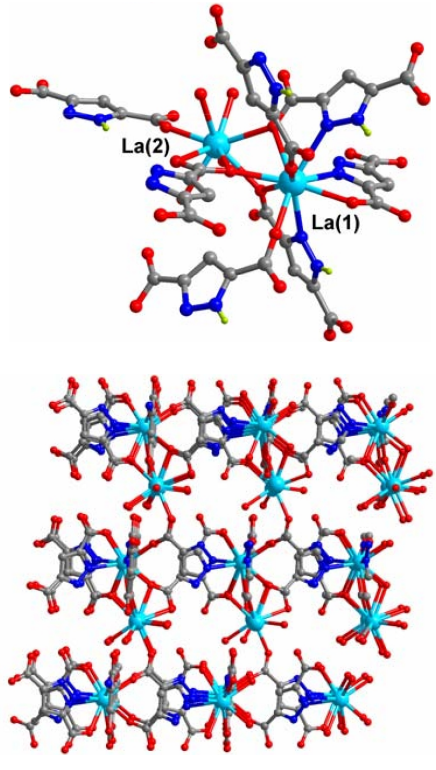

Fig. 5 (color online). Views of the coordination geometry around La(III) (a) and the three-dimensional structure (b) of compound **12**. La (turquoise), O (red), N (blue), C (gray) and H (lime).

common due to the large and variable coordination numbers and consequently more complicated structures [42, 43]. Lanthanide coordination polymers **12** – **17** prepared by hydrothermal synthesis, feature 2D and 3D structures [44]. The compounds $[Ln_2(Hpdc)_3(H_2O)_4] \cdot 2H_2O$ [*Ln* = La (**12**) and Ce (**13**), H_3pdc = 3,5-pyrazoledicarboxylic acid] were synthesized by heating the mixtures of $Ln(NO_3)_3 \cdot 6H_2O$, H_3pdc and H_2O in the molar ratio of 1 : 1 : 2222 in an 23 mL acid digestion bombs at 150 °C for 3 d. Compounds **12** and **13** feature three-dimensional structures containing nine-coordinated metal centers (Fig. 5). There are two crystallographically independent lanthanide sites in **12** and **13**: *Ln*1 site is coordinated to six $Hpdc^{2-}$ ligands, among which three $Hpdc^{2-}$ ligands afford one carboxylate oxygen atom and an adjacent nitrogen atom each while the remaining three $Hpdc^{2-}$ ligands only afford one single oxygen atom for coordination; *Ln*2 is coordinated to three oxygen atoms from three monodentate $Hpdc^{2-}$ ligands, two oxygen atoms from one bidentate $Hpdc^{2-}$ ligand and four oxygen atoms from four H_2O molecules. Thus, the $Hpdc^{2-}$ ligands have three different coordination modes in the structure.

The europium compound $[Eu_2(Hpdc)_3(H_2O)_6]$ (**14**) was prepared under similar experimental conditions as for **12** and **13**. It exhibits a rare clay-like double layer structure (Fig. 6). In **14**, the Eu(III) centers are eight-coordinated with a square-antiprismatic geometry to three oxygen atoms from three separate $Hpdc^{2-}$ ligands, one oxygen atom and an adjacent nitrogen atom from a fourth $Hpdc^{2-}$ ligand, and three oxygen atoms afforded by three H_2O molecules. The existence of two types of $Hpdc^{2-}$ ligands results in a unique double-layer structure. Hydrogen bonding interactions are found between the double layers.

The erbium compound $[Er(Hpdc)(H_2pdc)(H_2O)_2]$ (**15**) was prepared in an acidic environment (pH = 1). Hydrated $Er(NO_3)_3$, H_3pdc, HNO_3 and H_2O (molar ratio: 1 : 1 : 1 : 1111) were reacted in a 23 mL acid digestion bomb at 150 °C for 3 d, and the pure product was collected after washing and drying in air. The lutetium compound $[Lu(Hpdc)(H_2pdc)(H_2O)_2]$ (**16**) was prepared by a similar procedure as used for **12** – **14**. Structure analyses showed that both **15** and **16** have novel single-layered structures (Fig. 7), in which the lanthanide atoms are all eight-coordinated with $Hpdc^{2-}$, H_2pdc^{-} and H_2O, respectively. There are two types of ligands involved in the coordination:

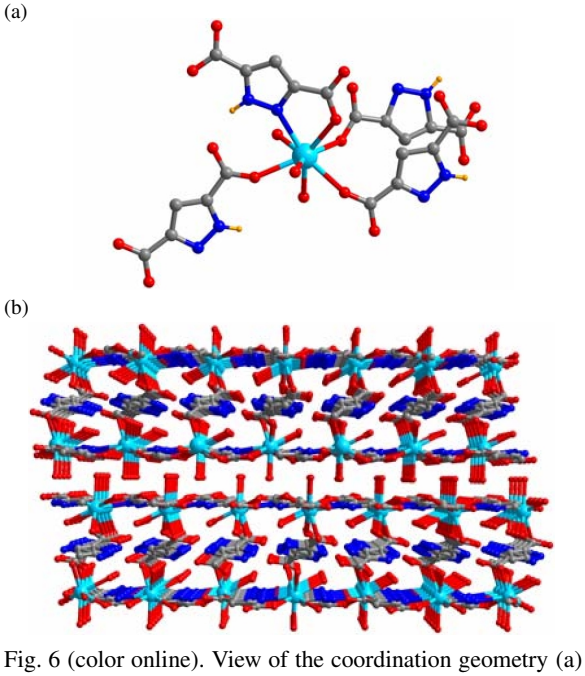

Fig. 6 (color online). View of the coordination geometry (a) and the double layer clay-like structure (b) of compound **14**. Eu (turquoise), O (red), N (blue), C (gray) and H (lime).

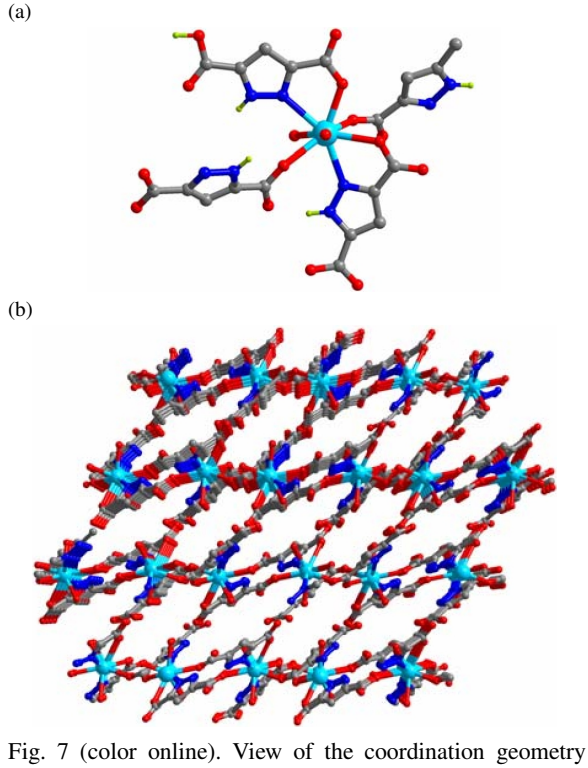

Fig. 7 (color online). View of the coordination geometry (a) and the single-layer structure (b) of compound **15**. Er (turquoise), O (red), N (blue), C (gray) and H (lime).

mono-deprotonated H_2pdc^- and dual-deprotonated $Hpdc^{2-}$. In the mono-deprotonated H_2pdc^- ligand, only one carboxylate group can participate in the coordination, whereas both carboxylate groups of the dual-deprotonated $Hpdc^{2-}$ ligands are available for coordination. By adjusting the level of deprotonation of the ligand, the double-layered erbium compound $[Er_2(Hpdc)_3(H_2O)_6]$ (**17**) that contains the dual-deprotonated $Hpdc^{2-}$ ligand only was successfully isolated at pH = 5. This study indicates that the formation of products under hydrothermal conditions is easily affected by the acidity (or basicity) of the reaction medium. Structures with different coordination geometry and dimensionality may be achieved by controlling the pH value. In addition, the effect of lanthanide contraction is also found in the formation of these lanthanide coordination polymers, in accordance with the decreasing trend of coordination numbers from nine only for La(III) and Ce(III) compounds, to both nine and eight for Eu(III) compounds, and to eight only for Er(III) and Lu(III) compounds.

Using the same ligand H_3pdc, further research revealed that, when lanthanide ions are replaced by transition metal ions, three deprotonation processes (including the proton at a pyrazole nitrogen atom) may be controlled by the acidity of the reaction mixture (Scheme 2) [45].

$$\mathbf{H_3pdc} \underset{+H}{\overset{-H}{\rightleftharpoons}} \mathbf{H_2pdc^-} \underset{+H}{\overset{-H}{\rightleftharpoons}} \mathbf{Hpdc^{2-}} \underset{+H}{\overset{-H}{\rightleftharpoons}} \mathbf{pdc^{3-}}$$

Scheme 2. Protonation and deprotonation processes in H_3pdc.

The 3D cadmium coordination polymer $[Cd(Hpdc)(H_2O)]$ (**18**) was assembled by hydrothermal reactions of $Cd(NO_3)_2$ (0.2 mmol), $H_3pdc \cdot H_2O$ (0.4 mmol) and H_2O (10 mL) in a Teflon-lined bomb at 150 °C for 12 d (pH = 2.5 in the final solution). Yellowish block-like crystals of **18** were collected in high yields (98 %). In compound **18**, the Cd(II) centers are seven-coordinated with adopting a pentagonal bipyramidal configuration (Fig. 8a). The resultant structure contains solely $Hpdc^{2-}$ ligands coordinating the Cd(II) ions. Zigzag ribbons are found extending parallel to the *c* axis formed through connecting neighboring Cd(II) ions with single bridging $Hpdc^{2-}$. The inter-ribbon connections further result in the formation of a three-dimensional structure. When the pH value of the reaction solution was changed from 2.5 to 4 by introducing Et_3N (0.5 mmol), reactions of $Cd(NO_3)_2$ (0.5 mmol) and H_3pdc (0.25 mmol) in H_2O (10 mL) using the same temperature and time period gave a new 3D coordination network $[Cd_3(pdc)_2(H_2O)_2]$ (**19**) as pale-yellow plate crystals. Though all Cd(II) ions are six-coordinated in **19**, two crystallographically independent metal sites are found in the structure (Fig. 8b). The ligands in **19** are in the fully deprotonated form of pdc^{3-} rather than $Hpdc^{2-}$ found in **18**. It is quite apparent that the pH value is an important factor affecting the structure formation during hydrothermal reactions and can serve as a controlling factor in the rational synthesis of novel coordination polymers.

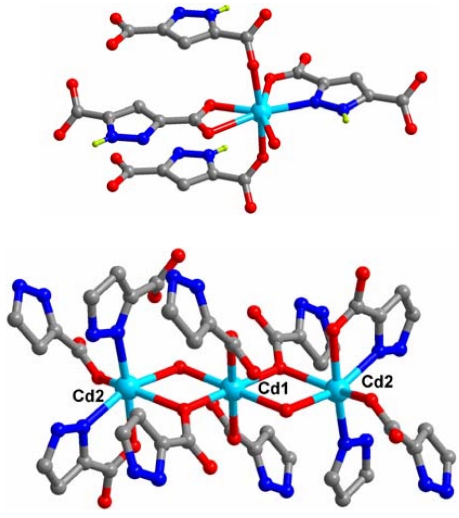

Fig. 8 (color online). View of the coordination geometry of compounds **18** (a) and **19** (b). Cd (turquoise), O (red), N (blue) and C (gray).

By controlling the pH value of the reaction [46], the hydrothermal synthesis with alkaline earth salts [47] or their hydroxides with the H_3pdc ligand gave several new coordination polymers exhibiting different dimensionality. To yield compound $[Ca(Hpdc)(H_2O)_4] \cdot 2H_2O$ (**20**) [48], a mixture of $CaCl_2$ (0.2 mmol), H_3pdc (0.1 mmol) and deionized water (10 mL) was heated in a Teflon-lined bomb at 150 °C for 3 d. After evaporating the resultant colorless solution (pH = 2.5), colorless polyhedral crystals were collected by filtration and washing (68 % yield). $[Ca(Hpdc)(H_2O)_4] \cdot H_2O$ (**21**) was similarly obtained by evaporating the hydrothermal reaction solution (pH = 5.0) of $CaCl_2$ (0.2 mmol), H_3pdc (0.1 mmol), Et_3N (0.2 mmol), and water (10 mL) at 150 °C for 3d. Compounds **20** and **21** have one-dimensional structures consisting of infinite zigzag

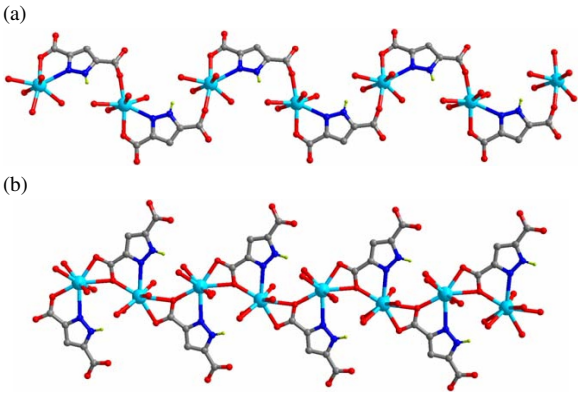

Fig. 9 (color online). One-dimensional chains in compounds **20** (a) and **21** (b). Ca (turquoise), O (red), N (blue), C (gray) and H (lime).

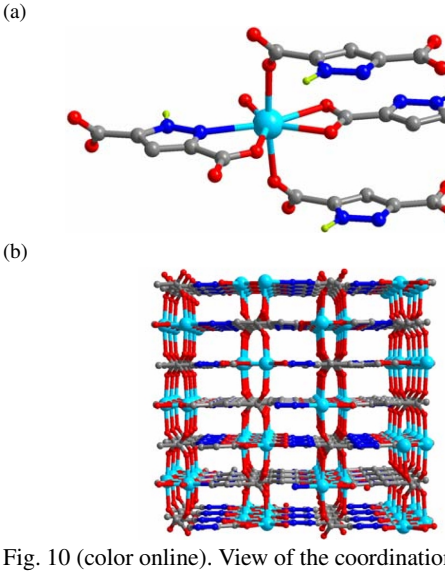

Fig. 10 (color online). View of the coordination environment (a) and the three-dimensional framework (b) of compound **22**. Ca (turquoise), O (red), N (blue), C (gray) and H (lime).

chains constructed by tetra-aqua-calcium units and bridging $Hpdc^{2-}$ ligands (Fig. 9). A hydrothermal reaction of $CaCl_2$ (0.2 mmol), H_3pdc (0.1 mmol) and Et_3N (0.4 mmol) in 10 mL H_2O (pH = 9.0) at 150 °C for 3 d gave colorless column-like crystals of $[Ca(Hpdc)(H_2O)]$ (**22**) (86 % yield). Using $Ca(OH)_2$ (0.5 mmol) in place of $CaCl_2$, the reaction with H_3pdc (0.5 mmol) in 10 mL H_2O (pH = 11.5) under the same experimental conditions (except pH) can also produce compound **22**. Different from compounds **20** and **21**, **22** exhibits a three-dimensional structure and is isostructural to the aforementioned compound **18** (Fig. 10). A comparison of the structures of **20**, **21** with **22** reveals that the connectivity numbers of the ligands in these compounds increase from μ_3 and μ_4, up to μ_6, consistent with the increasing degree of deprotonation of the ligands with the higher pH of the corresponding reaction mixtures.

Alkaline earth metals with a larger radius were also investigated. The strontium and barium compounds $[Sr(Hpdc)(H_2O)]$ (**23**), $[Ba(H_2pdc)_2(H_2O)]\cdot 2H_2O$ (**24**) and $[Ba(Hpdc)(H_2O)]$ (**25**) were prepared by adopting similar hydrothermal reaction procedures as for **20** – **22**

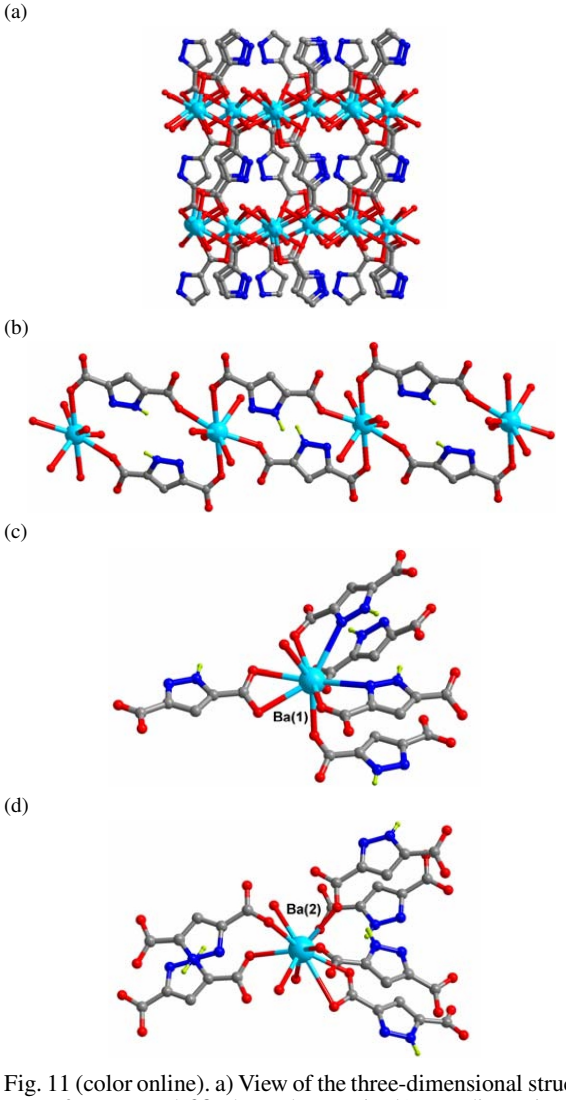

Fig. 11 (color online). a) View of the three-dimensional structure of compound **23** along the *c* axis; b) one-dimensional ribbon in compound **24**; c) and d) view of the coordination geometry of the two crystallographically independent barium sites in compound **25**. Sr/Ba (turquoise), O (red), N (blue), C (gray) and H (lime).

but at different pH values. A study on compounds **23** – **25** (Fig. 11) has revealed similar trends in the connectivity numbers of the ligands, as well as in the resultant dimensionality of the structures. The same studies on alkaline earth metals have also shown that at lower pH values the metals tend to coordinate to water molecules, correspondingly limiting their ability to form structures with higher dimensionality.

It is a general observation in the aforementioned investigations on rare-earth, transition, post-transition, and alkaline earth metals that the acidity of the reaction media plays a crucial role in the structure formation under hydrothermal conditions. Increasing pH leads to higher connectivity of the ligands, and correspondingly to the formation of structures of higher dimensionality.

When pyridine is introduced into the reaction, competition with water in coordination to metal centers is often observed [49]. The one-dimensional chains of compound $[Co(bpdc)(H_2O)_2]$ (**26**) (bpdc = biphenyldicarboxylate) can be easily obtained by the reaction of $Co(NO_3)_2$ and $Na_2(bpdc)$ in aqueous solution [50]. The Co^{II} ions in compound **26** are bridged by four μ_2-H_2O and two *trans* μ_2-bpdc ligands to form 1D chains along the *c* axis (Fig. 12a). Starting from this precursor, several structural transformations are observed in mild chemical reactions. When compound **26** was immersed into a pyridine/water (2 : 1) solution, single crystals of $[Co(bpdc)(py)_2(H_2O)_2] \cdot 2py$ (**27**) formed very quickly. Compound **27** also exhibits a one-dimensional chain structure, in which the Co^{II} ions are bonded to two μ_2-bpdc *via* monodentate carboxylic oxygen atoms, but has two terminal water and two pyridine molecules (Fig. 12b). Hydrogen bonds are found between the hydrogen atoms of coordinated water molecules and uncoordinated carboxylic oxygen atoms. The reaction of $Co(NO_3)_2$ (0.5 mmol) and H_2bpdc (0.25 mmol) in pyridine/water (v : v, 1 : 1) solution in a digestion bomb at 120 °C for 3 d gave single crystals of the compound $[Co(bpdc)(py)_2] \cdot H_2O$ (**28**). Compound **28** features a non-interpenetrating two-dimensional network, which is constructed by Co^{II} ions being interconnected through chelating and bridging monodentate and bidentate $bpdc^{2-}$ ligands (Fig. 12c). Compound **26** can also be obtained by immersion of compounds **27** or **28** in water, suggesting that interconversion between seemingly unrelated structures can occur under mild conditions.

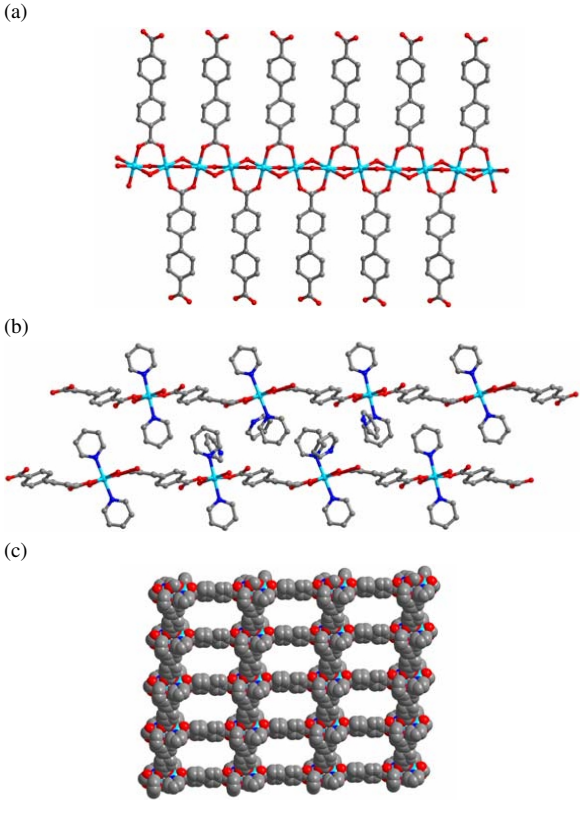

Fig. 12 (color online). a) View of a single chain extending along the *c* axis in **26**; b) the stacking pattern of the single chains in **27**; c) space-filling model of the non-interpenetrating two-dimensional network of compound **28**. Co (turquoise), O (red), N (blue) and C (gray).

A similar structural transformation phenomenon is also observed in rare earth coordination polymers [51]. The reaction of hydrated $Er(NO_3)_3$ (0.075 g), H_2bdc (0.036 g) (H_2bdc = terephthalic acid) in H_2O (10 mL) and EtOH (1 mL) mixed solvent was carried out in a 23 mL acid digestion bomb at 160 °C for 3 d to

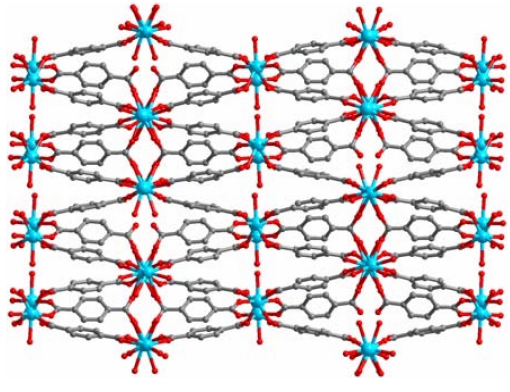

Fig. 13 (color online). Perspective view of the crystal structure of **29** along the *a* axis. Er (turquoise), O (red) and C (gray).

yield $[Er_4(bdc)_6] \cdot 6H_2O$ (**29**) as pink crystals. Treating a sample of **29** by first heating at 300 °C under nitrogen gas, followed by exposure to saturated water vapor for 2 h, gave compound $[Er_2(bdc)_3] \cdot 4H_2O$ (**30**), which is isostructural to $[Tb_2(bdc)_3] \cdot 4H_2O$ reported by Yaghi *et al.* [42]. Compounds **29** and **30** both feature condensed three-dimensional network structures. Three types of coordination polyhedra are found for Er^{III} ions in compound **29** (Fig. 13). However, in compound **30** only a single type of dodecahedral coordination geometry is adopted by the Er^{III} ions.

Two isomorphic phases of the one-dimensional compounds [α-$ZnCl_2$(bpy)] (**31**) and [β-$ZnCl_2$(bpy)] (**32**) were assembled by a hydrothermal synthetic method [52]. Compound **31** was prepared by the reactions of $ZnCl_2$ (1 mmol), bpy (bipyridine, 1 mmol) and H_2O (2 mL) in a Teflon-lined autoclave at 170 °C for 4 d. Using different stoichiometry of the same reactants with reduced concentrations ($ZnCl_2$ 0.1 mmol, bpy 0.3 mmol, H_2O 8 mL) gave compound **32**. One-dimensional zigzag chains are found in the structures of **31** and **32**. Zn^{II} ions feature tetrahedral geometry that involves two bridging bpy ligands and two terminal chloride ions (Fig. 14). The main difference between the two structures is that one mirror plane passes through the Zn and N atoms in compound **32** while a 2-fold axis exists at the Zn atoms in compound **31**.

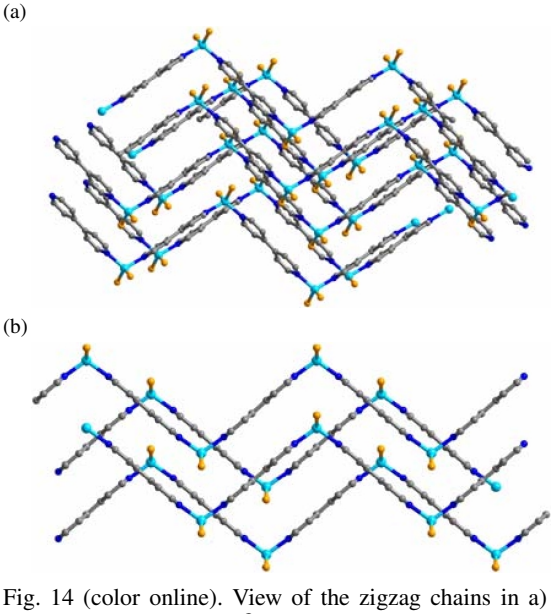

Fig. 14 (color online). View of the zigzag chains in a) α-$ZnCl_2$(bpy) (**31**) and b) β-$ZnCl_2$(bpy) (**32**). Zn (turquoise), Cl (orange), N (blue) and C (gray).

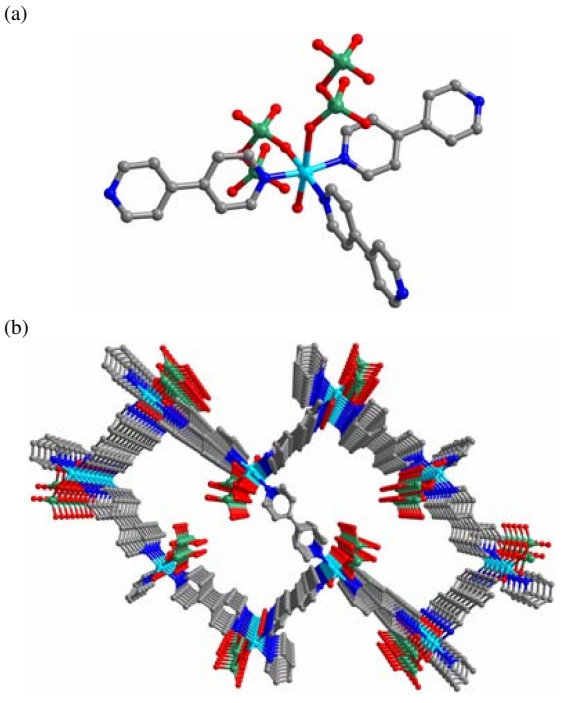

Fig. 15 (color online). View of a) the coordination environment around the Cu^{II} sites, and b) the $4^6 6^4$ 3D network found in compound **33**. Cu (turquoise), Cr (green), O (red), N (blue) and C (gray).

In compound $[Cu(bpy)_{1.5}(Cr_2O_7)] \cdot H_2O$ (**33**), the $Cr_2O_7^{2-}$ anion was found acting as an effective secondary ligand to bridge Cu centers in a 3D structure [53]. Compound **33** was synthesized in a hydrothermal reaction of $Cu(NO_3)_2 \cdot 3H_2O$, bpy, $K_2Cr_2O_7$ and H_2O in the ratio of 1 : 1 : 0.5 : 5555 at 150 °C for 3 d. In the structure, Cu centers are all six-coordinated to three nitrogen atoms from three bpy ligands, two oxygen atoms from two $Cr_2O_7^{2-}$ anions and an oxygen atom from a water molecule (Fig. 15). Cu atoms are connected with bpy ligands to form a 2D Cu-bpy network, which is further extended to a unique 3D structure having $4^6 6^4$ topology by the bonding between the Cu centers and the $Cr_2O_7^{2-}$ anions. Large 1D channels are found along the *a* axis with a cross-section of the windows measured as 11.2 × 22.0 Å^2. Two identical networks are also found interlocking in the structure to present two-fold interpenetration, avoiding the formation of large open space.

Hydrogen-bonded three-dimensional networks $[M(H_2pdc)_2(H_2O)_2] \cdot 2H_2O$ (M = Mn, Fe, Co, Ni, Zn) were also prepared by hydrothermal reactions [54]. In a typical procedure, heating of $Co(NO_3)_2 \cdot 6H_2O$

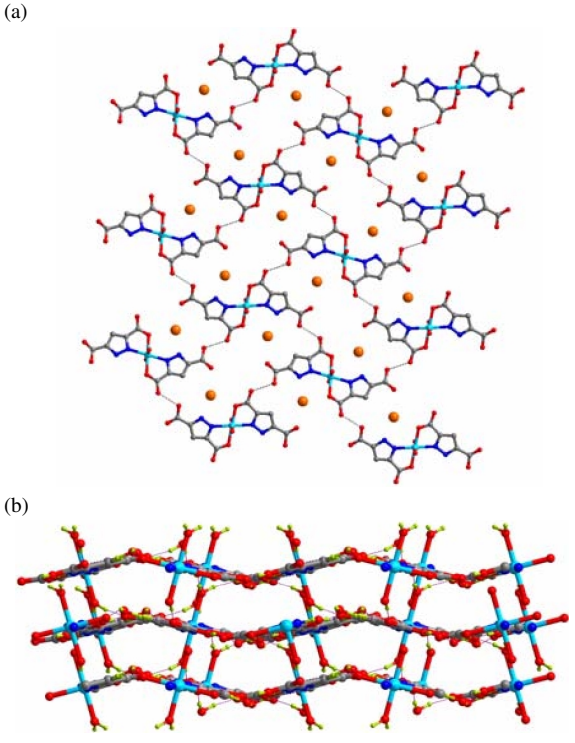

Fig. 16 (color online). a) View of the basket-weave-like, two-dimensional hydrogen-bonded network in compound **34** (the large yellow balls represent the two water molecules); b) view of the hydrogen-bonded 3D network of compound **34**. Co (turquoise), O (red), N (blue), C (gray) and H (lime).

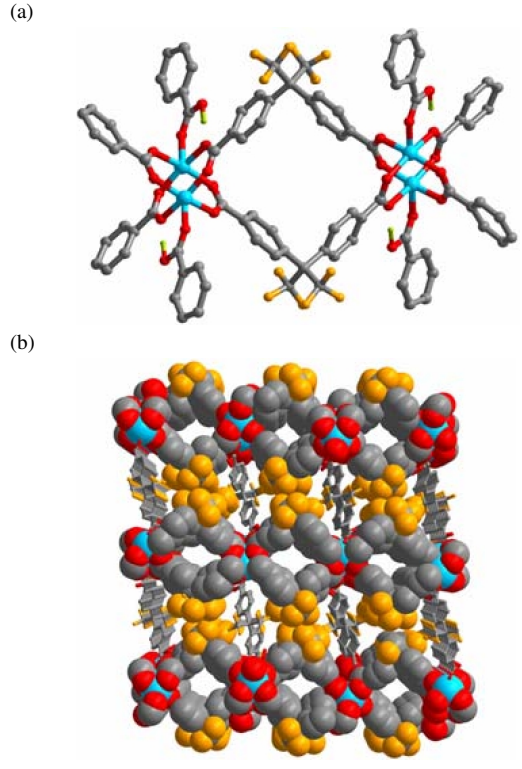

Fig. 17 (color online). a) Secondary building unit and cross section of a single microtube, and b) the three-dimensional packing of **36**. Cu (turquoise), O (red), C (gray), F (orange) and H (lime).

(0.25 mmol) and H_3pdc (0.5 mmol) in 10 mL H_2O (pH = 1.5) at 150 °C for 3 d gave beige column-like crystals of $[Co(H_2pdc)_2(H_2O)_2] \cdot 2H_2O$ (**34**). In compound **34**, each Co^{II} ion is six-coordinated to two sets of oxygen and adjacent pyrazole nitrogen atoms from two separate H_2pdc^- ligands and two H_2O molecules. Basket-weave-like 2D networks are found through strong hydrogen bonds between two neighboring H_2pdc^- ions in compound **34** (Fig. 16). Adjacent layers are further interconnected through hydrogen bonding between the coordinated water molecules and the 3,5-pyrazoledicarboxylate ions. Upon heating of these hydrogen-bonded compounds, all four water molecules in the structures can be removed. This process is accompanied with distinct color changes. After re-immersing the formed amorphous samples in water the original 3D structure can be recovered. Such a reversible structural interconversion process can be explained by breakage and reformation of the hydrogen bonding network. Dissolution of dehydrated **34** (6 mg) in methanol (3 mL) leads to the transformation to another supramolecular compound $[Co_4(Hpdc)_4(py)_{12}]$ (**35**) upon addition of pyridine (2 mL).

The microporous metal-organic framework [Cu(hfipbb)$(H_2$hfipbb$)_{0.5}$] (**36**) was prepared by hydrothermal reaction of $Cu(NO_3)_2 \cdot 3H_2O$ (0.12 mmol) and H_2hfipbb (0.5 mmol) (H_2hfipbb = 4,4′-(hexafluoroisopropylidene)-bis(benzoic acid)) in 5 mL water at 125 °C for 3 d [55]. Blue column-like crystals of compound **36** were collected after washing (DMF, 10 mL × 3) and vacuum drying (92 % yield). The three-dimensional structure of compound **36** (Fig. 17) is built upon paddle-wheel-like di-copper secondary building units (SBUs), which are formed by two Cu(II) ions sharing four carboxylate groups from four hfipbb^{2-} ligands (Cu–Cu distance: 2.645 Å). These SBUs are interconnected by hfipbb ligands to form an ondulating 2D network with 4^4 topology. Further interconnection of adjacent 2D layers through the binding of monodentate H_2hfipbb ligands to apical positions of the di-cooper paddle-wheels give the three-

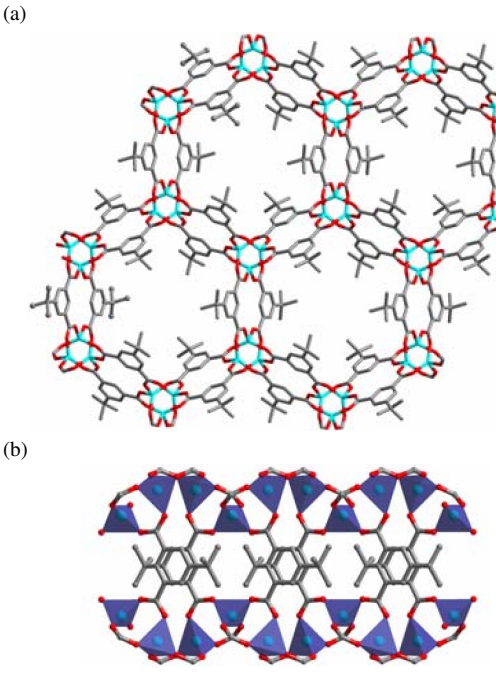

Fig. 18 (color online). a) Crystal structure of **37** showing the hexagonal close-packed 1D open channels along the *c* axis; b) view of the channel wall (ZnO_4 shown as a polyhedron). Zn (turquoise), O (red) and C (gray).

dimensional framework. A two-fold interpenetration is found in the structure, resulting in small microchannels ($\sim 3.5 \times 3.5$ Å^2, excluding the van de Waals radius of carbon) and larger cages ($\sim 5.1 \times 5.1$ Å^2) inside. TGA measurement has shown a guest-free framework for compound **36**, and a solvent-accessible volume of 11.6 % has been calculated by PLATON.

Compound [Zn(tbip)] (**37**) (tbip = 5-*tert*-butyl isophthalate) is another guest-free microporous coordination metal-organic framework [56]. **37** was synthesized by hydrothermal reaction of a mixture of $Zn(NO_3)_2 \cdot 6H_2O$ (0.66 mmol), H_2tbip (0.66 mmol), H_2O (13 mL) and ethylene glycol (3 mL) at 180 °C for 3 d. In the structure, Zn^{II} centers adopt tetrahedral coordination geometry by linking four $tbip^{2-}$ ligands (Fig. 18a). Adjacent zinc nodes are bridged by two carboxylate groups to generate a 3_1 helical chain with a pitch of 7.977 Å along the crystallographic *c* axis. Neighboring chains are interconnected through $tbip^{2-}$ ligands with the closest interchain distance of 7.212 Å, resulting in a 3D structure possessing hexagonal close-packed 1D open channels along the *c* axis. The diameter of the channel is reduced to 4.5 Å (excluding the van der Waals radius of hydrogen) due to the methyl groups protruding into the channel. Strong π-π interactions *via* a slipped π-stacking mode are found between the phenyl rings that form the channel walls (Fig. 18b). Compared with compound **36**, a larger freely accessible volume of 17.7 % of compound **37** is calculated by PLATON, which can be attributed to a more effective packing.

Solvothermal reactions in non-aqueous solvents

As widely as hydrothermal reactions have been used in the preparation of coordination network materials, non-aqueous solvents have also been commonly employed in the synthesis of MOF compounds. *N*,*N*′-Dimethylformamide (DMF) is one of the most common organic solvents used in these reactions due to its very good solubilizing capability for both the organic ligands and the inorganic metal salts.

Coordination networks containing multiporphyrin groups are particularly interesting due to their special electron distribution characters [57]. To construct a metalloporphyrin structure, a solvothermal synthesis strategy was used to improve the solubility of the free-base *meso*-tetra(4-pyridyl)porphyrin (H_2TPyP) ligand [58]. Heating a DMF (3 mL) solution of ferrocene (0.54 mmol) and H_2TPyP (0.24 mmol) in a Teflon-lined bomb at 150 °C for 5 d and washing the product with ethanol and diethyl ether gave two phases having the same composition: the main phase being the dark-red cubic crystals of α-[Fe(TPyP)] (**38**) (Fig. 19) and a minor phase being the red plate-like crystals of β-[Fe(TpyP)] (**39**). The Fe^{II} ions in both compounds are six coordinated with four N atoms from pyrrole moieties of the porphyrin ligand at equatorial

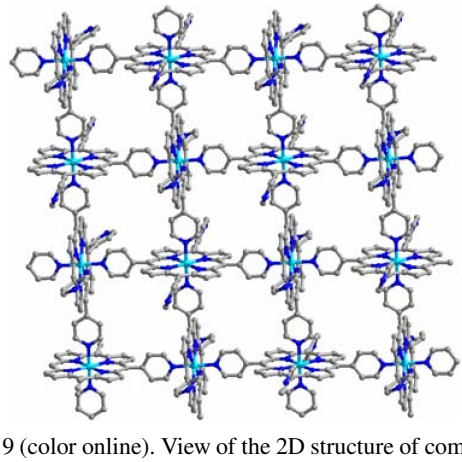

Fig. 19 (color online). View of the 2D structure of compound **38** along the *a* axis. Fe (turquoise), N (blue) and C (gray).

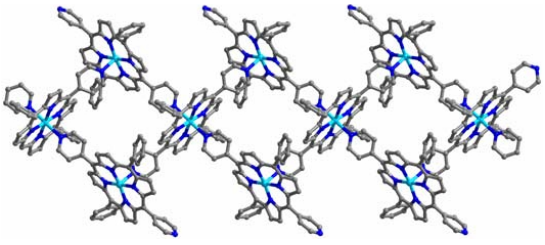

Fig. 20 (color online). View of the 1D coordination array in compound **40**. Co (turquoise), N (blue) and C (gray).

positions, and two pyridine N atoms from two adjacent porphyrin molecules at the two axial positions. Such a coordination configuration results in a two-dimensional paddle-wheel-like pattern with all neighboring porphyrin molecules mutually perpendicular. Single crystal analyses of compounds **38** and **39** revealed the different packing sequences: $\cdots$ABAB$\cdots$ in **38** and $\cdots$ABCDABCD$\cdots$ in **39**.

Another 1D metalloporphyrin polymer $[Co_3(DPyP)_3] \cdot 4DMF$ (**40**) was produced by using a *trans meso*-bifunctional porphyrin, 5,25-dipyridyl-10,20-diphenylporphyrin (H_2DPyP) [59]. Pink crystals of compound **40** were crystallized by solvothermal reactions of $Co(NO_3)_2$ with H_2DPyP in DMF at 130 °C. Structure analysis of compound **40** revealed a novel 1D infinite array of tetranuclear metalloporphyrin cages adjoined by the coordination of pyridyl nitrogen atoms to Co(II) (Fig. 20). There are two types of the metalloporphyrin found in the network, occupying the node and corner positions of the cages, respectively. The Co(II) ions in the nodal porphyrin ligands are six-coordinated while those in the porphyrin ligands occupying the corner positions are five-coordinated.

Porous three-dimensional materials, especially those having recyclable framework structures, are highly desirable due to their great potential in gas storage, separation and catalytic applications. The closely related 3D frameworks $[M_3(bpdc)_3(bpy)] \cdot 4DMF \cdot H_2O$ **41**(Co) and **42** (Zn) [60, 61] were prepared from a nonporous 1D precursor $[M(bpdc)(H_2O)_2] \cdot H_2O$ (M = Co, Zn) (the aforementioned **26**). In a typical reaction, a mixture of compound **26** (0.3 mmol) and bpy (0.1 mmol) in DMF (10 mL), sealed in a Teflon-lined bomb and heated at 150 °C for 3 d, gave rise to deep-purple columnar crystals of compound **41** (95 % yield). **41** can also be obtained by the solvothermal reaction of $Co(NO_3)_2$, H_2bpdc and bpy ligand in DMF at 150 °C for 3 d. The structure of compound **41** (Fig. 21) features unique

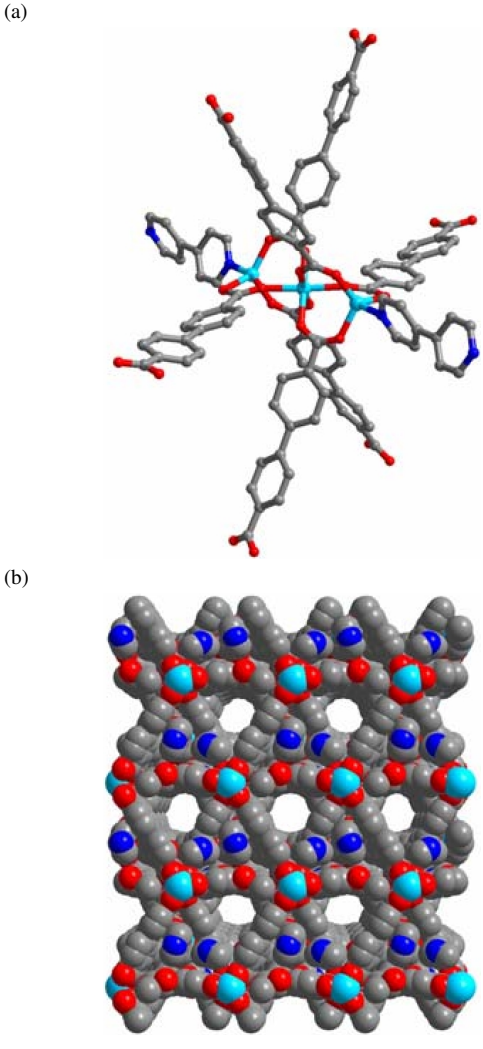

Fig. 21 (color online). The $[Co_3(bpdc)_6(bpy)_2]$ building unit (a) and the side view of the one-dimensional channels (b) in **41**. Co (turquoise), O (red), N (blue) and C (gray).

tri-nuclear SBUs, $[Co_3(COO)_6]$, which contain two crystallographically independent cobalt centers. The octahedrally coordinated Co1 center is located on the two-fold rotational axis, and the two adjacent Co2 centers adopt a distorted trigonal bipyramidal geometry. Each of the Co1–Co2 pairs is connected by two μ_2 and one μ_3 oxygen atoms from three carboxylate groups. Adjacent $[Co_3(COO)_6]$ SBUs, which act as nodes in the structure of compound **41**, are interconnected through six $bpdc^{2-}$ ligands to form a 2D layer in the *ab* plane. Adjacent layers are interconnected by bpy as pillaring ligands coordinating to the terminal Co2 centers to generate a 3D framework.

Two-fold interpenetration of such networks completes the structure of **41**. Structure analysis also reveals 1D channels that can be viewed as large supercages (approximately 11 × 11 × 5 $Å^3$, excluding the van der Waals radius of the carbon atoms) connected through smaller triangular windows of a maximum effective dimension of about 8 Å. The calculated solvent-accessible pore volume of the compound is 42.4 % of the unit cell volume. Studies have shown that the 3D framework of compound **41** is readily broken down and converted back to the nonporous 1D precursor **26**, and such a structural interconversion is completely reversible.

Similar to **41**, the zinc compound **42** can also be prepared from the solvothermal reaction of its corresponding 1D precursor and bpy in DMF, or directly from the reaction of $Zn(NO_3)_2$, H_2bpdc and bpy in the molar ratio of 1 : 1 : 1 in DMF, as colorless columnar crystals. Crystal structure analysis has revealed that the structure of **42** is closely related to that of **41** with minor differences. In compound **42**, two terminal Zn centers of the tri-nuclear SBU are tetrahedrally coordinated instead of the five-coordination pattern found in **41**. However, this difference in coordination configuration of the Zn^{II} ions does not cause striking changes in the overall motifs and topology of the structure. The calculated free volume in **42** is 40.7 % of the unit cell volume, slightly lower than in **41**.

By replacing the terminal py with bridging bpy ligands, the 2D network of **28** can be extended to a new 3D porous framework [Co(bpdc)(bpy)] · 0.5DMF (**43**) in a solvothermal reaction [62]. **43** was synthesized by heating a mixture of **28** and bpy in the molar ratio of 1 : 4 in DMF (5 mL) at 120 °C for one day. Orange needle-like crystals of **43** were obtained in high yield (90 %). Single-crystal X-ray diffraction has revealed that compound **43** still contains the 2D motif found in **28** (Fig. 22). The bidentate bpy ligands interconnect the 2D motifs to form a pillared 3D network. Two of these pillared 3D networks, identical in structure, interpenetrate each other to generate an overall structure of **43** with rectangular-shaped 1D open channels (∼ 5.6 × 3.0 $Å^2$, excluding the van der Waals radius of carbon atoms) along the *a* axis. DMF molecules are found filling the channels in a head-to-tail fashion, which can be removed upon heating to give 28.6 % free voids in the unit cell volume.

Interpenetration is also found in another luminescent microporous metal-organic framework [Zn_2(bpdc)$_2$(bpee)] · 2DMF (**44**) (bpee = 1,2-bipyridylethene) [63]. By reacting a mixture of $Zn(NO_3)_2$ (0.3 mmol), H_2bpdc (0.3 mmol) and bpee (0.3 mmol) in DMF (15 mL) in a Teflon-lined autoclave at 165 °C for 3 d, colorless block-shaped crystals of **44** were formed (58 % yield). The structure of compound **44** contains dinuclear eight-membered ring-type secondary building units (Fig. 23). Each four-connecting node is linked to four other nodes by $bpdc^{2-}$ ligands to form the 2D 4^4 (brick-like) net. Two of such identical nets interpenetrate to generate a layer. Bpee ligands are coordinated to two Zn centers of adjacent layers to satisfy the tetrahedral coordination configuration of each Zn center, and act as pillars interconnecting the layers to the overall 3D structure. Parallelogram-shaped 1D open channels run along the *b* axis with a window size around 5.0 × 7.0 $Å^2$ (excluding the van der Waals

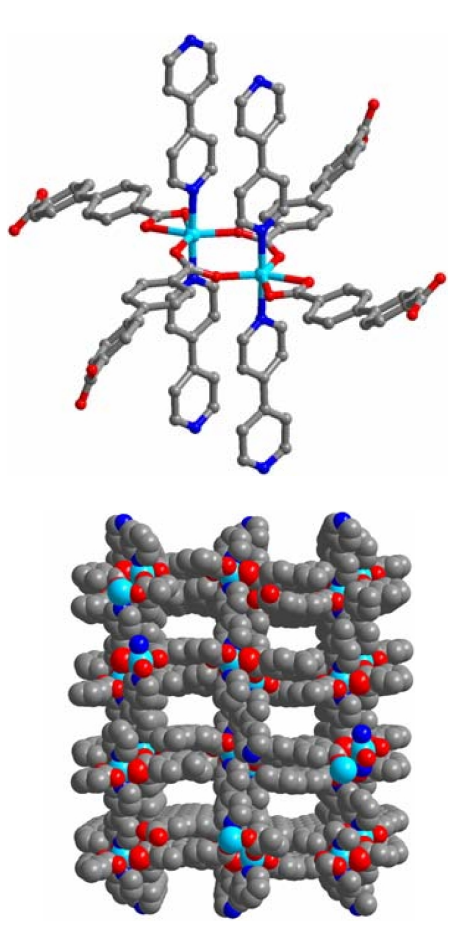

Fig. 22 (color online). The [Co_2(bpdc)$_4$(bpy)$_2$] building unit (a) and the catenated network with rectangular-shaped 1D channels (b) in **43**. Co (turquoise), O (red), N (blue) and C (gray).

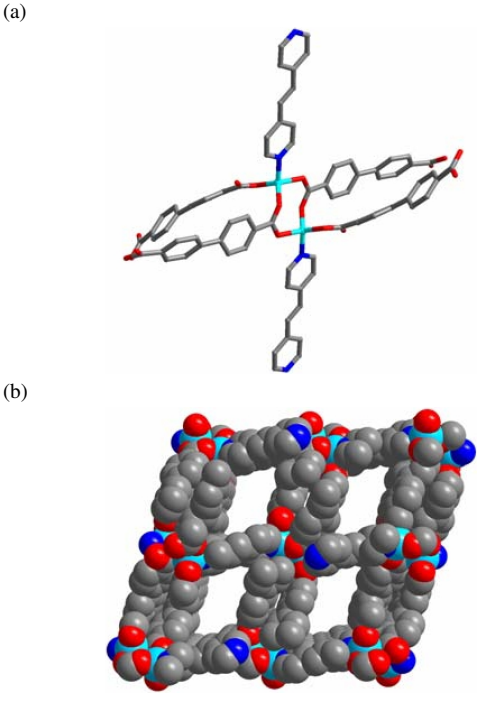

Fig. 23 (color online). The di-zinc secondary building unit (a) and the overall 3D framework (b) of **44**. Zn (turquoise), O (red), N (blue) and C (gray).

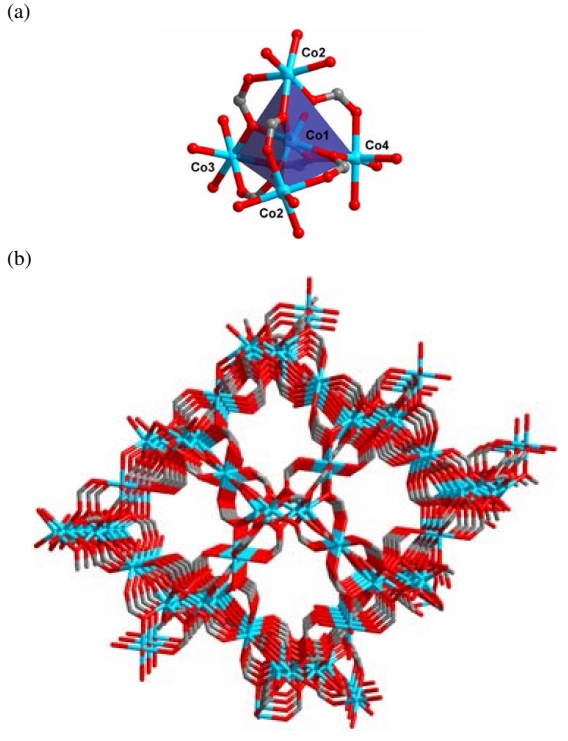

Fig. 24 (color online). The distorted penta-nuclear tetrahedron with Co1 residing in the center (a), and the perspective view of the overall structure of compound **45** along the *b* axis, showing the channels (b). Co (turquoise), O (red) and C (grey).

radius of the carbon atoms). 27.6 % of the unit cell volume is calculated as solvent-accessible volume in compound **44**.

Applications of porous framework materials, *e. g.* for gas storage and separation, require the sustainment of their structural integrity and porosity after removal of guest molecules. This remains a challenge partly due to the flexibility of extended organic ligands that are commonly employed to induce the formation of highly porous materials. Conversely, employing relatively shorter and more rigid ligands, such as formate, may yield more robust frameworks. Pink block-like single crystals of $[Co_3(HCOO)_6] \cdot DMF$ (**45**) were obtained by reaction of $Co(NO_3)_2$(1.4 mmol) and formic acid (97 %, 2.8 mmol) in DMF (20 mL) in a Teflon-lined bomb at 100 °C for 2 d [64]. An isostructural manganese compound $[Mn_3(HCOO)_6] \cdot DMF$ (**46**) and a nickel compound $[Ni_3(HCOO)_6] \cdot DMF$ (**47**) can also be prepared in a similar way. Compound **45** crystallizes in the monoclinic space group $P2_1/n$. Four crystallographically independent Co^{II} centers (the occupation factors of Co3 and Co4 are 0.5), six formate anions and one guest DMF molecule are found in the asymmetric unit of structure **45** (Fig. 24). The Co^{II} centers are all six-coordinated to oxygen atoms from separate formate ligands with distorted octahedral geometry. Among the four different Co^{II} centers, Co1 is located at the center of a distorted tetrahedron formed by Co2, Co3, Co4 and another Co2 atoms at the four apexes. Six formate ligands connect each of the Co^{II} centers at the apex in *syn/anti* mode along the edges of the tetrahedron, with one oxygen atom from each formate ligand also binding to the central Co1 atom in *syn* mode. The three-dimensional framework of compound **45** is built through apex-sharing of these Co1-centered $CoCo_4$ tetrahedron, which can be simplified by connecting all tetrahedral nodes into a distorted diamond-like network. One-dimensional zigzag channels (~ 5 – 6 Å in size) filled with DMF guest molecules are observed along the *b* axis. Based on the calculation of PLATON, 30.9 % of the unit cell volume can be used for other guests upon removal of the DMF.

One implication of using extended organic linkers to induce the formation of highly porous materials is that interpenetration of two or more iden-

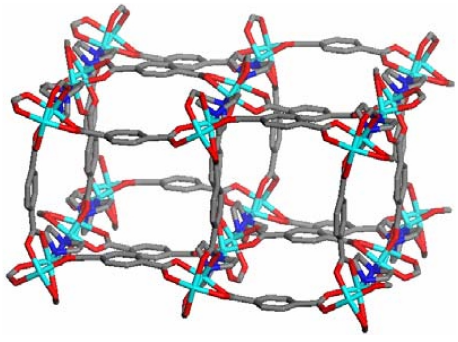

Fig. 25 (color online). View of the framework of compound **48**. Zn (turquoise), O (red), N (blue) and C (gray).

tical frameworks often results in low porosity. One possible solution to prevent interpenetration is to use bulky molecular species such as triethylenediamine (ted) [65]. $[Zn(bdc)(ted)_{0.5}] \cdot 2DMF \cdot 0.2H_2O$ (**48**) was crystallized from a solvothermal reaction mixture of $Zn(NO_3)_2$ (0.60 mmol), H_2bdc (0.61 mmol) and ted (0.32 mmol) in 15 mL of DMF kept at 120 °C for 2 d [66]. Colorless block-shaped crystals were isolated after washing with DMF and drying in air (83 % yield). The isostructural copper compound $[Cu(bdc)(ted)_{0.5}] \cdot 2DMF \cdot 0.2H_2O$ (**49**) was also prepared under similar conditions. Compound **48** crystallizes in the tetragonal crystal system with space group *P*4/*ncc*. The structure of **48** consists of paddle-wheel $Zn_2(COO)_4(ted)_2$ SBUs, which are linked by bdc ligands within the layer to form a 2D net (Fig. 25). The 2D nets are further linked by ted pillars to give rise to a 3D framework with three-dimensionally interconnected pores. The 3D porous structure contains two types of interlacing channels with the window size of the channels along the *c* axis at around 7.5 × 7.5 $Å^2$ and those along the *a* or *b* axes at around 4.8 × 3.2 $Å^2$ (excluding the van der Waals radius of the carbon atoms). The free volume calculated by PLATON is 58.4 % of the unit cell volume for **48**.

While aromatic carboxylate ligands are commonly employed in constructing porous coordination framework materials because of their good directionality in coordination and their mechanical rigidity, aliphatic carboxylate ligands are rarely found useful due to the lack of such properties. A few exceptions exist, in which rigid aliphatic ligands are used [67, 68]. For example, the aliphatic ligand H_2bodc (H_2bodc = bicycle[2.2.2]octane-1,4-dicarboxylic acid) and the pillar ligand ted have both been employed in the construction of two new isostructural 3D

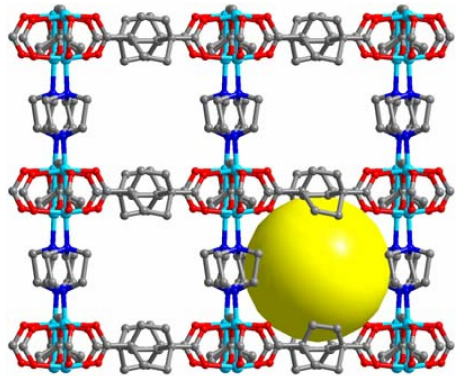

Fig. 26 (color online). The overall 3D structure of **51** (Co) with one cage being highlighted by the yellow sphere. Zn (turquoise), O (red), N (blue) and C (gray).

non-interpenetrating frameworks, $[Ni(bodc)(ted)_{0.5}]$ (**50**) and $[Co(bodc)(ted)_{0.5}]$ (**51**) (Fig. 26) [69]. The solvothermal reaction of $Ni(NO_3)_2$ (or $Co(NO_3)_2$) (0.64 mmol) with H_2bodc (0.58 mmol) and ted (1.41 mmol) in DMF (20 mL/0.1 mL conc. HNO_3 added) at 100 °C for 4 d yielded a crystalline powder of **50** (or **51**) in high yield. Structure analysis has revealed that compound **51** has a similar pillared layer structure as that of **48** and consists of paddle-wheel-like $Co(COO)_4$ SBUs. Calculation by PLATON shows that the three-dimensionally interconnected pores in **51** occupy about 49 % of the volume of the structure.

Apart from DMF, other organic solvents, such as methanol, ethanol, butanol, *etc.*, or their mixtures, can also be the solvents of choice for solvothermal reactions. Two novel zeolitic imidazolate frameworks (ZIFs) [70, 71], $[Zn(2\text{-}cim)_2] \cdot 2.1CH_3OH$ (**52**) and $[Zn(2\text{-}bim)_2] \cdot 0.16H_2O \cdot 0.16\ C_2H_5OH$ (**53**), containing 2-chloroimidzaole (2-cim) and 2-bromoimidazole (2-bim) as the ligands, respectively, were prepared using methanol as solvent [72]. The synthetic reaction for **52** was conducted in a glass vial containing a methanol (4 mL) solution of $Zn(NO_3)_2$ (0.4 mmol) and 2-cim (1 mmol). The solution was first homogenized by sonication, then covered and heated at 100 °C in an oven for 2 d, to give colorless polyhedral crystals of **52**. Similar to **52**, single crystals of **53** were obtained by reacting $Zn(NO_3)_2$ (0.4 mmol) and 2-bim (0.8 mmol) in ethanol (4 mL) for 2 d. Single-crystal X-ray diffraction has revealed that compounds **52** and **53** are isostructural to the recently reported ZIF-8 structure (with 2-methylimidazole as ligand) [70] (Fig. 27). In both structures, all Zn atoms are tetrahedrally coordinated by four N atoms from the imidazole (IM) ligands.

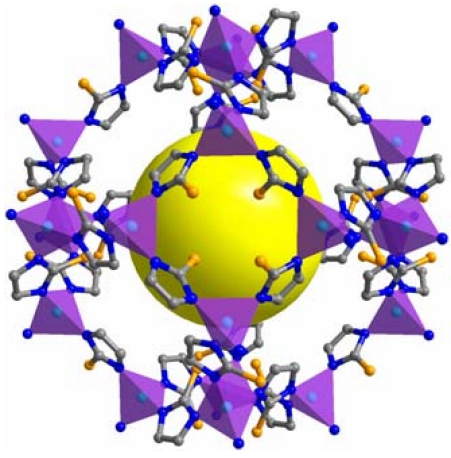

Fig. 27 (color online). View of the pore opening in compound **52**. Zn (turquoise), Cl (orange), N (blue) and C (gray).

Each IM ring bridges two Zn centers through its two N atoms at 1,3-positions to give Zn–IM–Zn angles close to 145°, which is coincident with the Si–O–Si angles of many zeolites. Both, **52** and **53** adopt the same expanded sodalite (*sod*) framework structure. The aperture sizes of the square windows in the truncated octahedral cages are almost negligible due to the blockage by the chlorine/bromine atoms. The cages are interconnected through the small openings delimited by H atoms on imidazolate ligands along the body-diagonal axes of the cubic crystal.

Solvothermal reactions in RTILs

Besides conventional organic solvents, room temperature ionic liquids (RTILs) can also be chosen as solvothermal reaction media. Due to their unique advantageous properties such as high thermal stability, air and moisture non-sensitivity, non-volatility, low reactivity, and templating and charge balancing ability, solvothermal synthesis in ionic liquids is specifically referred to as ionothermal synthesis [73]. The coordination polymer $[Cu(I)(bpp)]BF_4$ [bpp = 1,3-bis(4-pyridyl)propane] (**54**) was prepared by solvothermal reaction using the ionic liquid $[bmim][BF_4]$ (bmim = 1-butyl-3-methylimidazolium). $Cu(NO_3)_2 \cdot 3H_2O$ (0.05 mmol), bpp (0.05 mmol) and 0.1 mL of $[bmim][BF_4]$ were sealed in a glass tube and heated at 140 °C for 3 d to give compound **54** as column-like orange crystals [74]. Unlike those compounds obtained by other synthetic approaches, compound **54** shows a different structure: each Cu(I) ion is coordinated to two nitrogen atoms from two bpp ligands to

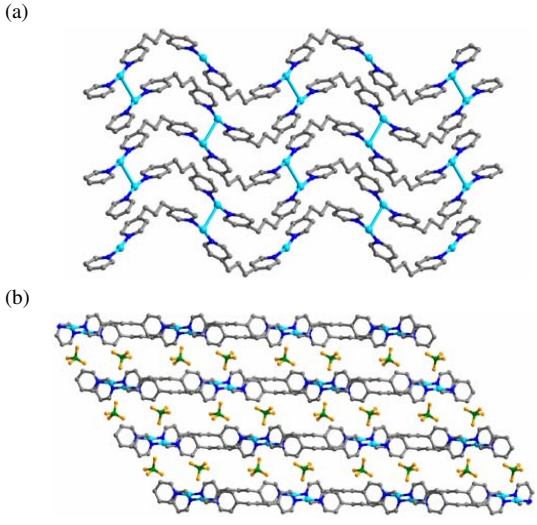

Fig. 28 (color online). View of **54** along the *c* axis showing a single layer of $[Cu(bpp)]^+$ (a) and along the *b* axis showing the parallel stacking of the $[Cu(bpp)]^+$ layers with BF_4^- anions located in between the layers (b). Cu (turquoise), N (blue), C (gray), F (orange) and B (green).

form a wave-like Cu-bpp chain. Weak Cu–Cu interactions are found between adjacent chains, extending the structure to two-dimensional (Fig. 28). The BF_4^- anions are found occupying the space between layers as charge-compensating species.

Properties and Multifunctionality

During the past decade, the chemistry of the infinite one-, two- and three-dimensional (1D, 2D, 3D) coordination frameworks has been an area of rapid growth. Tremendous interests, from physicists, chemists, and materials scientists, have been paid to the diversity and tunability of their structures and properties, as well as to their great potential in traditional and emerging new applications. Our on-going studies described herein exemplify the multifunctionality of such materials in hydrogen storage, hydrocarbon and other small gas sorption and separation, as well as sensing.

Hydrogen adsorption

Porous materials, particularly porous three-dimensional frameworks that we discuss here, have attracted increasing attention due to their ability for gas storage, especially for hydrogen storage. Hydrogen has been considered as a carbon-free clean energy carrier, which can be readily generated from water and hydrocarbons. Among the numerous viable

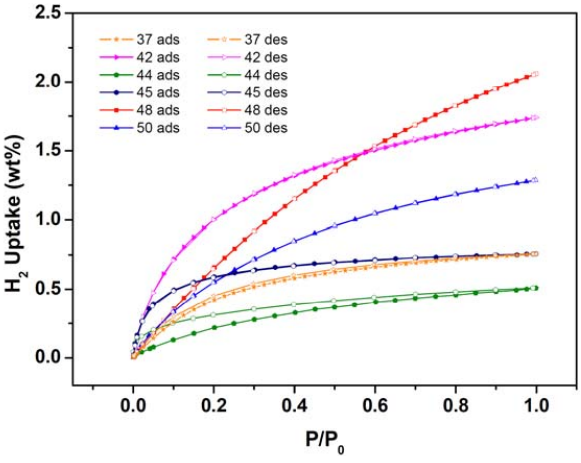

Fig. 29 (color online). H_2 adsorption-desorption isotherms of compounds, **37**, **42**, **44**, **45**, **48** and **50**.

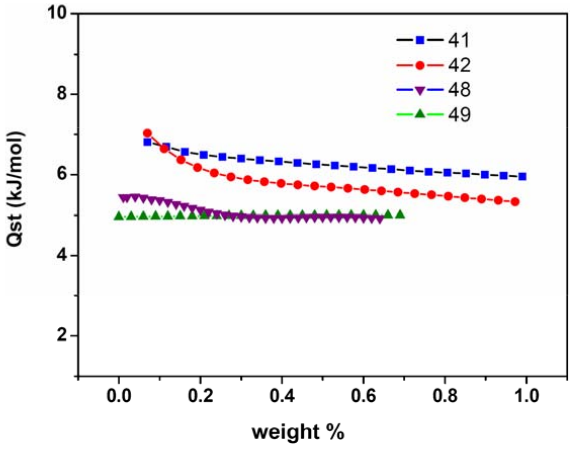

Fig. 30 (color online). Isosteric heats of H_2 adsorption for **41**, **42**, **48** and **49** as a function of the amount of hydrogen adsorbed.

hydrogen storage systems, porous metal coordination frameworks provide some unique advantages [75 – 78].

Thermal-gravimetric analysis of $[M(bdc)(ted)_{0.5}]$ (M = Zn **48**, Cu **49**) shows the high thermal stability of these two compounds even after removal of all guest solvent molecules. Physical adsorption of argon at low temperature (87 K) was used to further characterize the porosity of the frameworks. The pore size distributions of **48** and **49** were calculated from Ar adsorption isotherms at 87 K using the Horvath-Kawazoe (HK) method, showing that both materials have a very similar pore size distribution of around 7.8 Å, consistent with the values determined by the structure analysis. Brunauer-Emmett-Teller (BET) specific surface areas of 1794 and 1461 $m^2\ g^{-1}$, and total pore volumes of 0.65 and 0.52 $cm^3\ g^{-1}$ for **48** and **49**, respectively, were also obtained from the argon adsorption results.

The hydrogen sorption properties of **48** and **49** were investigated at 77 and 87 K (Fig. 29). Their hydrogen adsorption-desorption isotherms were recorded as a function of relative pressure (P/P_0) in the range of 10^{-4} to 1 atm. There is no hysteresis observed in the isotherms. The Zn structure (**48**) shows a higher H_2 uptake ability than the Cu structure (**49**) over the whole region. The adsorbed amount of hydrogen corresponds to 2.1 and 1.8 wt.-% at 77 K and 1 atm, 1.2 and 1.1 wt.-% at 87 K and 1 atm for **48** and **49**, respectively. An analysis of the isosteric heats of adsorption (Q_{st}) shows the extent of sorbent-sorbate interactions between hydrogen and the frameworks. The Q_{st} values range roughly from 4.9 to 5.4 kJ mol^{-1} for **48** for the H_2 coverage of 0.01 to 0.6 wt.-%, and are around 5.0 kJ mol^{-1} for **49** for the H_2 coverage of 0.02 to 0.7 wt.-%.

The structures of $[Co_3(bpdc)_3(bpy)]$ (**41**) and $[Zn_3(bpdc)_3(bpy)]$ (**42**) were also chosen for a study of their hydrogen adsorption properties [60, 61]. Based on the argon adsorption isotherms on compounds **41** and **42**, the Horvath-Kawazoe (H-K) pore size analysis showed that two types of pores, including ultramicropores (with diameters of $\sim$ 7 Å) and supermicropores (with diameters of $\sim$ 15 Å for **41** and 10 Å for **42**) exist in both compounds, in excellent agreement with the crystallographic data. Analysis of the argon adsorption isotherms gave BET surface areas of 922 and 792 $m^2\ g^{-1}$ for **41** and **42**, respectively. The total pore volumes were estimated to be 0.38 $cm^3\ g^{-1}$ for **41** and 0.33 $cm^3\ g^{-1}$ for **42**. The capacities of hydrogen uptake at 77 K and 1 atm are 1.98 and 1.74 wt.-% (1.48 and 1.32 wt.-% at 87 K) for **41** and **42**, respectively. Compound **41** shows a higher hydrogen uptake capacity than **42** at all pressure levels, and the calculated isosteric heats of adsorption (Q_{st}) at 77 and 78 K are also higher for **41** than for **42**, suggesting a stronger adsorbent-adsorbate interaction in **41** (Fig. 30). It is worth noting that the very high densities of the adsorbed H_2 (0.053 $cm^3\ g^{-1}$ and 0.052 $cm^3\ g^{-1}$ at 77 K and 1 atm for **41** and **42**, respectively) at the experimental conditions are nearly comparable to those of liquid H_2 (*e. g.* 0.053 $cm^3\ g^{-1}$ at 30 K and 8.1 atm).

The H_2 adsorption at 25 °C on the guest-free framework compound **36** was performed by charging with hydrogen at increasing pressures up to 48 atm with monitoring the weight change by a pulse mass analyzer

[55]. Compound **36** shows an almost linearly increasing hydrogen uptake up to 1.0 wt.-% at 48 atm. This value is comparable with the best performing single-walled carbon nanotubes (SWNTs). As a further comparison, MOF-5, which has larger pore dimensions of $\sim 7.7 \times 7.7$ Å^2, was also studied [79]. Despite that the accessible pore volumes of MOF-5 are 6.6 times higher than those of **36** (76.8 % to 11.6 %), the hydrogen uptake capacity (1.65 % at 48 atm) of MOF-5 is only 1.8 times that of compound **36**. This suggests that the pore volume is not the sole factor that determines the H_2 uptake capacity. Other factors, including the pore size and the specific surface area, should be considered as well. Thus tailoring the pore size to fit the molecular diameter of H_2 may serve as a working strategy to enhance the H_2 storage capacity, in addition to other strategies, such as impregnation, catenation, using lighter metals, and inclusion of unsaturated metal sites, that are all also under active investigation [80].

Small gas separation

Guest-free metal organic frameworks generally possess ultramicropores ($<$ 7 Å) and exhibit high adsorption selectivity to small gas molecules, which can be used for their separation from other gases [81]. For example, a study of compound **37** (Zn(tbip)) has shown the potential for separation of MeOH from water and dimethyl ether (DME) [56]. Due to the very hydrophobic nature, compound **37** exhibits essentially zero adsorption ability for water ($< \sim 1$ mg g^{-1} at $P/P^0 = 0.65$) but high adsorption ability for methanol, 110 mg g^{-1} at 24.5 °C and 90 Torr MeOH ($P/P^0 = 0.73$). The MeOH adsorption isotherms exhibit the typical capillary condensation adsorption behavior with very little of MeOH adsorbed up to 40 Torr (less than ~ 3 mg g^{-1}) and a very sharp increase in adsorption beyond 40 Torr. Isotherms at various temperatures show that the condensation point of MeOH shifts to higher P/P^0 with increasing temperature by around 4.7 Torr °C^{-1} (Fig. 31a). The adsorption isotherms of DME and MeOH indicate that compound **37** has the potential to selectively adsorb DME at conditions of T and P below the capillary condensation point of MeOH (Fig. 31b). In addition, in the adsorption of the binary gases of DME and MeOH a temperature increase of a few degrees shifts the capillary condensation point of MeOH to higher pressure, resulting in desorption of the majority of the MeOH adsorbed and of a relatively small amount of DME. This suggests that temperature

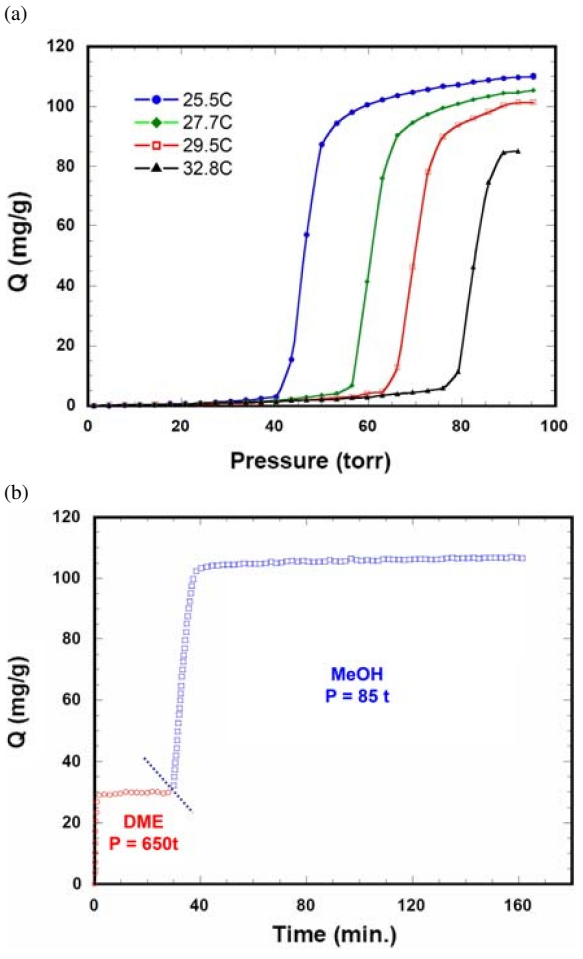

Fig. 31 (color online). MeOH adsorption isotherms at different temperatures (a) and adsorption of DME at 30 °C followed by MeOH adsorption in compound **37** as a function of time (b).

can play a critical role in the separation of DME and MeOH.

Compounds **48** and **49** exhibit similar, but much more efficient MeOH adsorption performance, 520 mg g^{-1} at 25 °C and 60 Torr. The capillary condensation adsorption behavior could also be observed in both MeOH and EtOH adsorption studies, but not for DME. This difference can be attributed to the existence of H-bonding between frameworks and the alcohol molecules, which is absent for DME. Because of the high hydrophobic surface of **48** and **49**, adsorption of only ~ 6 mg g^{-1} of water was recorded at $P/P^0 = 0.42$, which is less than the adsorption capacity (> 400 mg g^{-1}) for MeOH, EtOH and DME. Our study also indicated that the hydrocarbons with hydrophobic methyl

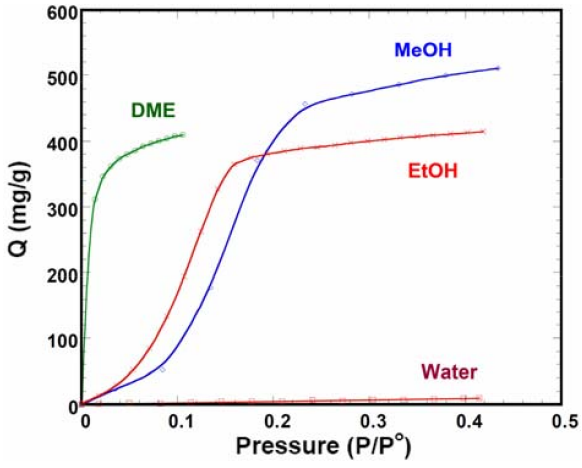

Fig. 32 (color online). Methanol, ethanol, dimethyl ether and water adsorption isotherms for compound **48** at 30 °C.

groups can be easily separated from water in water-containing gas-phase mixtures (Fig. 32).

Hydrocarbon sorption and separation

In contrast to the enormous research efforts on small molecule (H_2, N_2, Ar, CO_2, CH_4, *etc.*) gas adsorption by metal-organic frameworks, the research on hydrocarbon adsorption and separation has been still quite limited [79, 82]. Considering the vast diversity and tunability of their frameworks and pore structures, in terms of pore size, shape and surface characteristics, porous metal-organic framework materials are also promising candidates for hydrocarbon adsorption and separation.

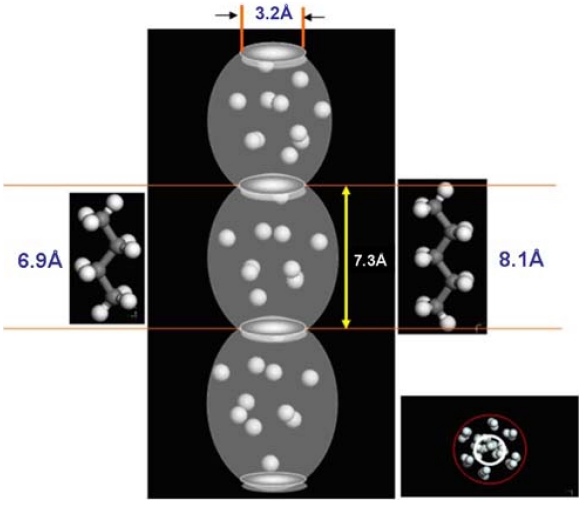

Fig. 33 (color online). A schematic view of the microchannel in compound **36** to show the sizes of the oval-shaped cages and the opening of the neck regions which are the critical factors for selective hydrocarbon adsorption.

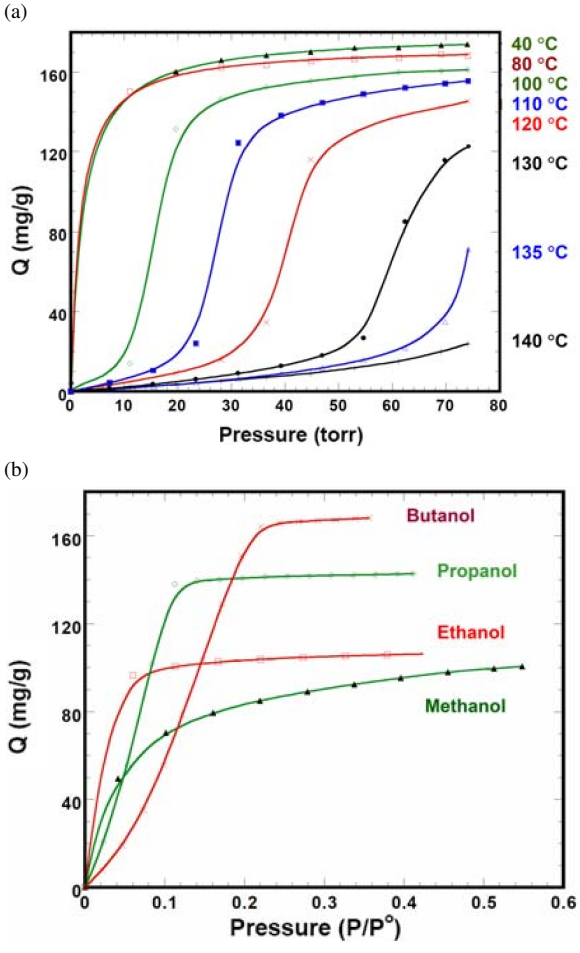

Fig. 34 (color online). Benzene adsorption isotherms at different temperatures (a) and light alcohol adsorption isotherms (b) for compound **45**.

Compound **36**, to the best of our knowledge, is the first material exhibiting the ability to separate normal C2–C4 olefins and alkanes from all higher branched alkanes and normal hydrocarbons [83]. In spite of its very small pore volume, compound **36** exhibits unique adsorption capacity for propane and butane over pentane or higher normal or branched hydrocarbons. This unusual property can be attributed to the special pore structure. The narrow channels in **36** can be viewed as alternating oval-shaped cages connected through narrow "neck" regions. This structural feature is better manifested by helium adsorption simulation (Fig. 33). The length of the large chamber ($\sim$ 7.3 Å) is just

longer than the length of *n*-C4 ($\sim$ 6.9 Å) molecules and shorter than *n*-C5 molecules (8.1 Å). The diameter of the "neck" regions is calculated as 3.2 Å (excluding the van der Waals radius of carbon), which rules out equilibrium positions for a normal alkane ($>$ *n*-C5) at the neck regions. However, the size of the neck is just large enough to allow the passage of normal alkanes, but not branched alkanes.

Compound $[Co_3(HCOO)_6]$ **45** and its hydrocarbon adsorption capacity and selectivity were systematically studied (Fig. 34) [64]. Benzene adsorption isotherms have shown that **45** can adsorb 3.94 molecules of benzene per unit cell, in agreement with the simulated result of 3.73 molecules per unit cell in the same temperature and pressure region. Both experimental data and simulations suggest a commensurate accommodation of benzene in the channels of **45**. Compared with benzene, the adsorption isotherms for toluene, ethylbenzene and *p*-xylene of **45** reveal that the number of molecules adsorbed per unit cell decreases monotonically for this series, which can be attributed to the increasing steric constraint and rigidity from toluene to ethylbenzene to *p*-xylene.

A study of the adsorption of light alcohols, from methanol to pentanol, has also demonstrated the controlling role of the channel structure of compound **45**. When the EtOH isotherm is already flat at 30 °C and high pressure, the isotherm for MeOH still has a significant positive slope in the same region, indicating the arrival of the adsorption limit for EtOH but not for MeOH. From the isotherms, EtOH as well as C3 and C4 alcohols, all have an adsorption maximum of 4 molecules per unit cell, suggesting the commensurate accommodation of these molecules in the channel of compound **45**. MeOH does not have this loading limit due to its smaller size. Adsorption isotherms also suggest that compound **45** has a higher affinity to EtOH over MeOH due to the CH_2 group interacting with the framework, which is consistent with the expected increase in the isosteric heats of adsorption.

A similar effect of commensurate pore shape-guest molecule accommodation is found in the propane adsorption by **45**. As a molecule of a length comparable to that of EtOH (5.84 Å *vs*. 5.64 Å), propane also has an adsorption limit of 4 molecules per unit cell, but for hexane with a size (10.20 Å) twice that of propane, the loading limit decreases to 2.1 molecules per unit cell, roughly $^1/_2$ that of propane. For most adsorbents studied, the isosteric heats of adsorption were essentially constant for the loading level, indicating that the adsorption is mainly controlled by the adsorbate-adsorbent interactions rather than adsorbate-adsorbate interactions.

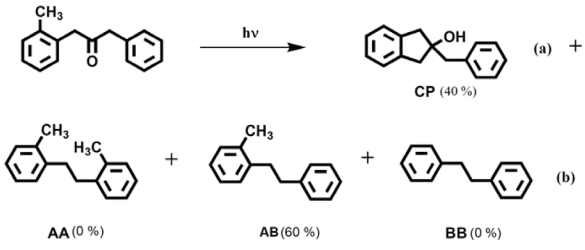

Scheme 3.

Ship-in-bottle synthesis

The well-defined pores in MOFs offer them great potential as hosts for size- and shape-selective reactions, such as "ship-in-bottle" synthesis [84]. In a "ship-in-bottle" reaction, synthesis is conducted within a framework containing an internal cavity (bottle) to give the product (ship) generally with high selectivity. The porosity and the unique 3D $\leftrightarrow$ 1D recyclable interconversion found in compound **41** make it an interesting "bottle" for special synthesis reactions [61]. Based on earlier work on the photochemistry of dibenzylketon (DBK) and derivatives inside a zeolite, *o*-MeDBK will undergo two photoreactions: (a) an intramolecular hydrogen abstraction followed by cyclization with formation of a cyclopentanol, **CP**, and (b) an α-cleavage followed by removal of carbon monoxide with the formation of a pair of hydrocarbon radicals, which further undergo geminate (product **AB**) or random combination (products **AA**, **AB**, and **BB**) (Scheme 3) [85]. When *o*-MeDBK is adsorbed by compound **41**, analysis has revealed that photolysis produces **CP** with 40 % yield in reaction (a) and **AB** with 60 % yield in reaction (b), and that both yields are much higher than those values found in a zeolites "ship". More importantly, direct extraction from the "broken bottle" with the structure conversion from 3D to 1D non-porous precursor releases the products to reach a 100 % mass balance. This study suggests the unique potential of the frameworks with certain pores or channels to serve as "smart" porous host for "ship-in-bottle" reactions or other syntheses.

Luminescence, sensing and detection

MOFs also offer a unique platform for the development of solid-state luminescent materials, and there

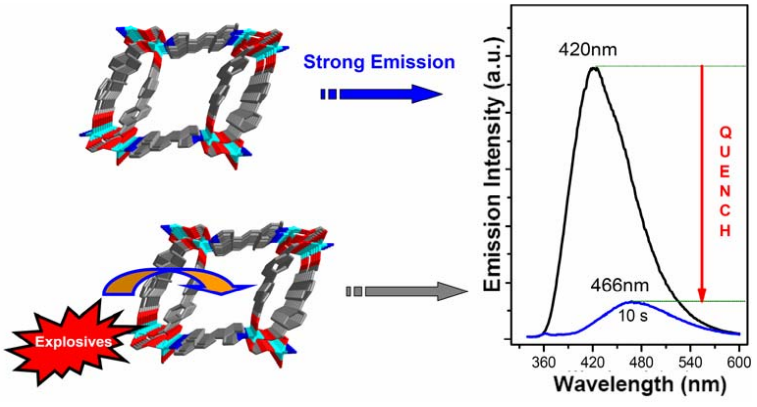

Fig. 35 (color online). A schematic illustration of the luminescence quenching of compound **44** induced by explosives.

have been reported numerous MOFs with interesting light emitting properties [86, 87]. The combination of the porous and luminescent nature of such materials endows them with the capability of transducing the host-guest chemistry to detectable signals, *e. g.* to changes of luminescence, making them promising candidates for sensing applications. The highly luminescent microporous metal-organic framework $[Zn_2(bpdc)_2(bpee)]$ (**44**) exhibits very fast and reversible quenching of its luminescence upon exposure to the vapors of electron-deficient compounds, *e. g.* DNT (2,4-dinitrotoluene) and DMNB (2,3-dimethyl-2,3-dinitrobutane) [63]. (Fig. 35). When a guest-free sample of **44** is exposed to equilibrated vapors of DNT or DMNB, very rapid (within 10 seconds) and close to complete fluorescence quench for both DNT ($\sim$ 85 %) and DMNB ($\sim$ 84 %) are recorded. There are also guest-dependent red-shifts of the fluorescence peaks accompanying the quenching process, indicative of guest-dependent interactions between the host framework and the analytes. More significantly, the photoluminescence of **44** can be fully recovered by simply heating the material at 150 °C for about one minute. Since DNT and DMNB are closely associated with high explosives, **44** might be used for fast and reversible detection of explosives. Previous studies on conjugated polymer thin films and other sensing materials have demonstrated that higher dimensionality may enhance sensitivity, because the excitons can be effectively quenched by increasing analyte binding sites through delocalization over the conjugated backbone ("molecular wire" effect), through interchain energy migration in the solid state, or through a highly organized molecular stacking structure [88]. Accordingly, the infinite three-dimensional framework structure of compound **44** with well-ordered π systems will facilitate quenching of the excitons through similar mechanisms.

Summary

In this review, we have presented the result of our work on the construction of coordination polymers carried out in the last decade. It has been shown how 1D, 2D and 3D networks are formed *via* hydrothermal and solvothermal synthesis methods, and the influences by numerous experiment parameters, such as solvent, pH, composition, temperature and pressure have been demonstrated. Our study has shown that the diversity of the networks is directly related to the choice of the vertex geometry and the organic linkers. Thus by choosing elaborately designed building blocks and organic ligands, the formation of coordination polymers with different topology and dimensionality can be controlled, and striking properties and multifunctionality, including those relevant to gas storage and separation, hydrocarbon adsorption and separation, catalysis and optical sensing, could be achieved.

Acknowledgements

The authors would like to thank the Department of Energy (DOE) for the financial support through Grant No. DE-FG36-08GO18139. We would also like to thank Dr. L. Pan, Dr. X. Y. Huang, Dr. D. H. Olson, Dr. J. Y. Lee, Dr. T. J. Emge, and A. J. Lan for their contributions.

[1] O. M. Yaghi, H. L. Li, C. Davis, D. Richardson, T. L. Groy, *Acc. Chem. Res.* **1998**, *31*, 474.
[2] G. Férey, *Chem. Soc. Rev.* **2008**, *37*, 191.
[3] S. Kitagawa, S. Kawata, *Coord. Chem. Rev.* **2002**, *224*, 11.
[4] B. F. Hoskins, R. Robson, *J. Am. Chem. Soc.* **1989**, *111*, 5962.
[5] C. Janiak, *Angew. Chem.* **1997**, *109*, 1499; *Angew. Chem., Int. Ed. Engl.* **1997**, *36*, 1431.
[6] A. J. Blake, N. R. Champness, P. Hubberstey, W. S. Li, M. A. Withersby, M. Schroder, *Coord. Chem. Rev.* **1999**, *183*, 117.
[7] A. Y. Robin, K. M. Fromm, *Coord. Chem. Rev.* **2006**, *250*, 2127.
[8] B. Moulton, M. J. Zaworotko, *Chem. Rev.* **2001**, *101*, 1629.
[9] S. R. Batten, R. Robson, *Angew. Chem.* **1998**, *110*, 1558; *Angew. Chem. Int. Ed.* **1998**, *37*, 1460.
[10] M. Eddaoudi, D. B. Moler, H. L. Li, B. L. Chen, T. M. Reineke, M. O'Keeffe, O. M. Yaghi, *Acc. Chem. Res.* **2001**, *34*, 319.
[11] S. Kitagawa, R. Kitaura, S. Noro, *Angew. Chem.* **2004**, *116*, 2388; *Angew. Chem. Int. Ed.* **2004**, *43*, 2334.
[12] C. Janiak, *Dalton Trans.* **2003**, 2781.
[13] D. Maspoch, D. Ruiz-Molina, J. Veciana, *Chem. Soc. Rev.* **2007**, *36*, 770.
[14] A. U. Czaja, N. Trukhan, U. Muller, *Chem. Soc. Rev.* **2009**, *38*, 1284.
[15] A. Y. Robin, K. M. Fromm, H. Goesmann, G. Bernardinelli, *Cryst. Eng. Comm.* **2003**, *5*, 405.
[16] B. F. Hoskins, R. Robson, *J. Am. Chem. Soc.* **1990**, *112*, 1546.
[17] R. Robson, *J. Chem. Soc., Dalton Trans.* **2000**, 3735.
[18] A. F. Wells, *Three-Dimensional Nets and Polyhedra*, Wiley, New York, **1977**.
[19] M. J. Zaworotko, *Chem. Soc. Rev.* **1994**, *23*, 283.
[20] M. J. Zaworotko, *Chem. Commun.* **2001**, 1.
[21] M. Fujita, Y. J. Kwon, S. Washizu, K. Ogura, *J. Am. Chem. Soc.* **1994**, *116*, 1151.
[22] M. C. Hong, Y. J. Zhao, W. P. Su, R. Cao, M. Fujita, Z. Y. Zhou, A. S. C. Chan, *Angew. Chem.* **2000**, *112*, 2586; *Angew. Chem. Int. Ed.* **2000**, *39*, 2468.
[23] S. Noro, S. Kitagawa, M. Kondo, K. Seki, *Angew. Chem.* **2000**, *112*, 2161; *Angew. Chem. Int. Ed.* **2000**, *39*, 2082.
[24] R. Kitaura, S. Kitagawa, Y. Kubota, T. C. Kobayashi, K. Kindo, Y. Mita, A. Matsuo, M. Kobayashi, H. C. Chang, T. C. Ozawa, M. Suzuki, M. Sakata, M. Takata, *Science* **2002**, *298*, 2358.
[25] R. Kitaura, K. Fujimoto, S. Noro, M. Kondo, S. Kitagawa, *Angew. Chem.* **2002**, *114*, 141; *Angew. Chem. Int. Ed.* **2002**, *41*, 133.
[26] C. Livage, N. Guillou, J. Marrot, G. Férey, *Chem. Mater.* **2001**, *13*, 4387.
[27] C. Serre, C. Férey, *J. Mater. Chem.* **2002**, *12*, 3053.
[28] H. Li, M. Eddaoudi, T. L. Groy, O. M. Yaghi, *J. Am. Chem. Soc.* **1998**, *120*, 8571.
[29] O. M. Yaghi, C. E. Davis, G. M. Li, H. L. Li, *J. Am. Chem. Soc.* **1997**, *119*, 2861.
[30] H. L. Li, C. E. Davis, T. L. Groy, D. G. Kelley, O. M. Yaghi, *J. Am. Chem. Soc.* **1998**, *120*, 2186.
[31] H. Li, M. Eddaoudi, M. O'Keeffe, O. M. Yaghi, *Nature* **1999**, *402*, 276.
[32] O. M. Yaghi, H. L. Li, *J. Am. Chem. Soc.* **1995**, *117*, 10401.
[33] J. Li, Z. Chen, R. J. Wang, D. M. Proserpio, *Coord. Chem. Rev.* **1999**, *192*, 707.
[34] X. M. Chen, M. L. Tong, *Acc. Chem. Res.* **2007**, *40*, 162.
[35] S. M. F. Lo, S. S. Y. Chui, L. Y. Shek, Z. Y. Lin, X. X. Zhang, G. H. Wen, I. D. Williams, *J. Am. Chem. Soc.* **2000**, *122*, 6293.
[36] J. L. C. Rowsell, O. M. Yaghi, *Microporous Mesoporous Mater.* **2004**, *73*, 3.
[37] G. Demazeau, *J. Mater. Sci.* **2008**, *43*, 2104.
[38] J. Y. Lu, B. R. Cabrera, R. J. Wang, J. Li, *Inorg. Chem.* **1998**, *37*, 4480.
[39] J. Y. Lu, B. R. Cabrera, R. J. Wang, J. Li, *Inorg. Chem.* **1999**, *38*, 4608.
[40] J. Y. Lu, M. A. Lawandy, J. Li, T. Yuen, C. L. Lin, *Inorg. Chem.* **1999**, *38*, 2695.
[41] M. A. Lawandy, X. Y. Huang, R. J. Wang, J. Li, J. Y. Lu, T. Yuen, C. L. Lin, *Inorg. Chem.* **1999**, *38*, 5410.
[42] T. M. Reineke, M. Eddaoudi, M. Fehr, D. Kelley, O. M. Yaghi, *J. Am. Chem. Soc.* **1999**, *121*, 1651.
[43] D. L. Long, A. J. Blake, N. R. Champness, C. Wilson, M. Schroder, *Angew. Chem.* **2001**, *113*, 2509; *Angew. Chem. Int. Ed.* **2001**, *40*, 2444.
[44] L. Pan, X. Y. Huang, J. Li, Y. G. Wu, N. W. Zheng, *Angew. Chem.* **2000**, *112*, 537; *Angew. Chem. Int. Ed.* **2000**, *39*, 527.
[45] L. Pan, X. Y. Huang, J. Li, *J. Solid State Chem.* **2000**, *152*, 236.
[46] L. F. Ma, L. Y. Wang, X. K. Huo, Y. Y. Wang, Y. T. Fan, J. G. Wang, S. H. Chen, *Cryst. Growth Des.* **2008**, *8*, 620.
[47] R. G. Harrison, O. D. Fox, M. O. Meng, N. K. Dalley, L. J. Barbour, *Inorg. Chem.* **2002**, *41*, 838.
[48] L. Pan, T. Frydel, M. B. Sander, X. Y. Huang, J. Li, *Inorg. Chem.* **2001**, *40*, 1271.
[49] O. M. Yaghi, G. M. Li, H. L. Li, *Nature* **1995**, *378*, 703.
[50] L. Pan, N. Ching, X. Y. Huang, J. Li, *Inorg. Chem.* **2000**, *39*, 5333.
[51] L. Pan, N. W. Zheng, Y. G. Wu, S. Nan, R. Y. Yang, X. Y. Huang, J. Li, *Inorg. Chem.* **2001**, *40*, 828.
[52] A. H. Fu, J. Y. Lu, X. Y. Huang, J. Li, *J. Alloys Compd.* **2001**, *319*, 89.

[53] L. Pan, N. Ching, X. Y. Huang, J. Li, *Chem. Commun.* **2001**, 1064.
[54] L. Pan, N. Ching, X. Y. Huang, J. Li, *Chem. Eur. J.* **2001**, *7*, 4431.
[55] L. Pan, M. B. Sander, X. Y. Huang, J. Li, M. Smith, E. Bittner, B. Bockrath, J. K. Johnson, *J. Am. Chem. Soc.* **2004**, *126*, 1308.
[56] L. Pan, B. Parker, X. Y. Huang, D. H. Olson, J. Lee, J. Li, *J. Am. Chem. Soc.* **2006**, *128*, 4180.
[57] R. K. Kumar, I. Goldberg, *Angew. Chem.* **1998**, *110*, 3176; *Angew. Chem. Int. Ed.* **1998**, *37*, 3027.
[58] L. Pan, S. Kelly, X. Y. Huang, J. Li, *Chem. Commun.* **2002**, 2334.
[59] L. Pan, X. Y. Huang, H. L. N. Phan, T. J. Emge, J. Li, X. T. Wang, *Inorg. Chem.* **2004**, *43*, 6878.
[60] J. Y. Lee, L. Pan, S. R. Kelly, J. Jagiello, T. J. Emge, J. Li, *Adv. Mater.* **2005**, *17*, 2703.
[61] L. Pan, H. M. Liu, X. G. Lei, X. Y. Huang, D. H. Olson, N. J. Turro, J. Li, *Angew. Chem.* **2003**, *115*, 560; *Angew. Chem. Int. Ed.* **2003**, *42*, 542.
[62] L. Pan, H. M. Liu, S. P. Kelly, X. Y. Huang, D. H. Olson, J. Li, *Chem. Commun.* **2003**, 854.
[63] A. J. Lan, K. H. Li, H. H. Wu, D. H. Olson, T. J. Emge, W. Ki, M. C. Hong, J. Li, *Angew. Chem.* **2009**, *121*, 2370; *Angew. Chem. Int. Ed.* **2009**, *48*, 2334.
[64] K. H. Li, D. H. Olsan, J. Y. Lee, W. H. Bi, K. Wu, T. Yuen, Q. Xu, J. Li, *Adv. Funct. Mater.* **2008**, *18*, 2205.
[65] D. N. Dybtsev, H. Chun, K. Kim, *Angew. Chem.* **2004**, *116*, 5143; *Angew. Chem. Int. Ed.* **2004**, *43*, 5033.
[66] J. Y. Lee, D. H. Olson, L. Pan, T. J. Emge, J. Li, *Adv. Funct. Mater.* **2007**, *17*, 1255.
[67] B. L. Chen, M. Eddaoudi, T. M. Reineke, J. W. Kampf, M. O'Keeffe, O. M. Yaghi, *J. Am. Chem. Soc.* **2000**, *122*, 11559.
[68] J. Kim, B. L. Chen, T. M. Reineke, H. L. Li, M. Eddaoudi, D. B. Moler, M. O'Keeffe, O. M. Yaghi, *J. Am. Chem. Soc.* **2001**, *123*, 8239.
[69] K. H. Li, J. Lee, D. H. Olson, T. J. Emge, W. H. Bi, M. J. Eibling, J. Li, *Chem. Commun.* **2008**, 6123.
[70] K. S. Park, Z. Ni, A. P. Cote, J. Y. Choi, R. D. Huang, F. J. Uribe-Romo, H. K. Chae, M. O'Keeffe, O. M. Yaghi, *Proc. Natl. Acad. Sci.* **2006**, *103*, 10186.
[71] R. Banerjee, A. Phan, B. Wang, C. Knobler, H. Furukawa, M. O'Keeffe, O. M. Yaghi, *Science* **2008**, *319*, 939.
[72] K. H. Li, D. H. Olson, J. Seidel, T. J. Emge, H. W. Gong, H. P. Zeng, J. Li, *J. Am. Chem. Soc.* **2009**, *131*, 10368.
[73] W. M. Reichert, J. D. Holbrey, K. B. Vigour, T. D. Morgan, G. A. Broker, R. D. Rogers, *Chem. Commun.* **2006**, 4767.
[74] K. Jin, X. Y. Huang, L. Pang, J. Li, A. Appel, S. Wherland, *Chem. Commun.* **2002**, 2872.
[75] N. L. Rosi, J. Eckert, M. Eddaoudi, D. T. Vodak, J. Kim, M. O'Keeffe, O. M. Yaghi, *Science* **2003**, *300*, 1127.
[76] B. L. Chen, N. W. Ockwig, A. R. Millward, D. S. Contreras, O. M. Yaghi, *Angew. Chem.* **2005**, *117*, 4823; *Angew. Chem. Int. Ed.* **2005**, *44*, 4745.
[77] J. L. C. Rowsell, E. C. Spencer, J. Eckert, J. A. K. Howard, O. M. Yaghi, *Science* **2005**, *309*, 1350.
[78] L. J. Murray, M. Dinca, J. R. Long, *Chem. Soc. Rev.* **2009**, *38*, 1294.
[79] M. Eddaoudi, J. Kim, N. Rosi, D. Vodak, J. Wachter, M. O'Keeffe, O. M. Yaghi, *Science* **2002**, *295*, 469.
[80] J. L. C. Rowsell, O. M. Yaghi, *Angew. Chem.* **2005**, *117*, 4748; *Angew. Chem. Int. Ed.* **2005**, *44*, 4670.
[81] R. Matsuda, R. Kitaura, S. Kitagawa, Y. Kubota, R. V. Belosludov, T. C. Kobayashi, H. Sakamoto, T. Chiba, M. Takata, Y. Kawazoe, Y. Mita, *Nature* **2005**, *436*, 238.
[82] B. L. Chen, C. D. Liang, J. Yang, D. S. Contreras, Y. L. Clancy, E. B. Lobkovsky, O. M. Yaghi, S. Dai, *Angew. Chem.* **2006**, *118*, 1418; *Angew. Chem. Int. Ed.* **2006**, *45*, 1390.
[83] L. Pan, D. H. Olson, L. R. Ciemnolonski, R. Heddy, J. Li, *Angew. Chem.* **2006**, *118*, 632; *Angew. Chem. Int. Ed.* **2006**, *45*, 616.
[84] N. J. Turro, *Acc. Chem. Res.* **2000**, *33*, 637.
[85] X. G. Lei, C. E. Doubleday, M. B. Zimmt, N. J. Turro, *J. Am. Chem. Soc.* **1986**, *108*, 2444.
[86] C. A. Bauer, T. V. Timofeeva, T. B. Settersten, B. D. Patterson, V. H. Liu, B. A. Simmons, M. D. Allendorf, *J. Am. Chem. Soc.* **2007**, *129*, 7136.
[87] M. D. Allendorf, C. A. Bauer, R. K. Bhakta, R. J. T. Houk, *Chem. Soc. Rev.* **2009**, *38*, 1330.
[88] S. W. Thomas, G. D. Joly, T. M. Swager, *Chem. Rev.* **2007**, *107*, 1339.